12-2016

Microstructure and Properties of Spark Plasma Sintered MoAlB Ceramics

Ting Lou
University of Nebraska-Lincoln, tlou3188@gmail.com

Microstructure and Properties of Spark Plasma Sintered MoAlB Ceramics

by

Ting Lou

A THESIS

Presented to the Faculty of

The Graduate College at the University of Nebraska

In Partial Fulfillment of Requirements

For the Degree of Master of Science

Major: Mechanical Engineering and Applied Mechanics

Under the Supervision of Professor Bai Cui

Lincoln, Nebraska

December, 2016

Microstructure and Properties of Spark Plasma Sintered MoAlB Ceramics

Ting Lou, M.S.

University of Nebraska, 2016

Advisor: Bai Cui

Molybdenum aluminum boride (MoAlB) is a ternary transition metal boride which has promising aeronautic and nuclear applications. It inheres excellent properties of the binary transitional metal borides (e.g., MoB, ZrB_2) such as high melting temperature, high hardness, and thermal conductivity. Besides, MoAlB is superior to MoB because: (1) the Al element provides an oxidation resistance at high temperatures; (2) its nanolaminated structure consisting of M-B layers with alternating Al layers results in a unique damage tolerance property. In this research, polycrystalline MoAlB have been successfully synthesized and simultaneously sintered using spark plasma sintering (SPS) from molybdenum boride (MoB) and aluminum (Al) powders. The SPS conditions have been optimized to obtain bulk samples with a high purity (>98 vol.%) and a high relative density (>97%). The microstructures have been characterized by X-ray diffraction and scanning electron microscopy. The mechanical property and oxidation behavior have been studied by using the Vickers indentation method and oxidation kinetics measurements, respectively.

Acknowledgments

First and foremost, I would like to appreciate my supervisor Dr. Bai Cui who give me this research about MoAlB ceramics which I am interested in. Without his instruction and patience, my research could not go well, and I also could not graduate successfully. I have learned a lot of knowledge and skills in Dr. Cui's group, so I feel proud.

I would also like to thank my committee members Dr. Michael Nastasi and Dr. Yongfeng Lu for taking time to correct my thesis. Besides, they give me valuable suggestions about my research.

Next, I am indebted to my colleagues Dr. Xueliang Yan, Meiyu Wang, Fei Wang, Ye Lin, and Qiaofeng Lu. They have helped and taught me to operate experimental devices; thereby, this master thesis can be finished successfully. I will never forget the days when I worked together with you.

Last but not least, I want to thank my friends, colleges, and families for their encouragement and support.

Table of Contents

List of Tables

List of Figures

Chapter 1: Introduction

1.1 Overview

Molybdenum aluminum boride (MoAlB) is a ternary transition metal boride which has promising aeronautic and nuclear applications. The MoAlB structure is molybdenum-boron (Mo-B) lattice interleaved by alternating layers of aluminum (Al). It has some special properties of resistance to oxidation in high temperature and a unique damage tolerance. Besides, it is inhering properties of binary transition metal borides (e.g., MoB, ZrB_2) such as high hardness, high melting temperature, electrical conductivity, chemical resistance, etc.

1.1.1 Overview of ceramics

Ceramics are defined as inorganic and nonmetallic compositions, which are comprising metallic and nonmetallic elements held by ionic and covalent bonds. General properties of ceramics are high hardness, high compression strength (Low tensile strength), low toughness, poor ductility, high melting point, high modulus of elasticity, poor thermal and electrical conductivity, good abrasive resistance, and good chemical resistance. Therefore, ordinary ceramics are widely used for wear resistant coating, heat insulator, chemical container, etc.

1.1.2 Binary transition metal borides

Binary transition metal borides (e.g., MoB, ZrB_2) are characterized by good thermal and electrical conductivity, and they also have some ordinary ceramics' properties such as high hardness, good abrasive resistance, poor ductility, etc. Thus, they are utilized as primary battery electrodes, wear resistant coatings, and high-temperature structural materials [1-4]. However, its application is limited because of poor oxidation resistance at high temperature and poor mechanical damage tolerance. For example, the Vickers hardness of single crystals of molybdenum diboride (MoB_2) on the (001) face is in the range 21.3 to 24.2 GPa, but the oxidation of the MoB_2 in the air begins at 500 ℃ reported by Okada *et al* [5]. Therefore, it results in manufacturing difficulties and applications limited at high temperature (>1000 ℃).

1.1.3 MAlB ceramics

Ternary transition metal borides MAlB-type has a transition metal boride (MB) lattice sandwiched by monolayers of aluminum (Al) element. Their special properties include: (1) the aluminum element provides an oxidation resistance at high temperatures; (2) its nanolaminated structure consisting of molybdenum-boron layers with alternating aluminum layers results in a unique damage tolerance property. Because of these special properties of MAlB ceramics, it can overcome the limitations of the binary transition metal borides, such as low fracture resistance and poor oxidation resistance in the high temperature oxidizing environment. Therefore, the

MAlB Ceramics are promising materials used for aeronautic and nuclear areas. Table 1.1 lists some properties between the ordinary ceramic, the binary transition metal boride and the ternary transition metal boride.

	Common Properties	Electrical and Thermal Conductivity	Damage Tolerance	Oxidation Resistance at High Temperature
Ordinary Ceramic	High hardness, high compressive strength, high melting point, high modulus of elasticity, good abrasive resistance, and good chemical resistance	Poor	Poor	Poor
Binary Transition Metal Boride		Good	Poor	Poor
Ternary Transition Metal Boride		Good	Good	Good

Table 1.1: Common and different properties of ordinary ceramic, binary transition metal boride and ternary transition metal boride

MoAlB belongs to the MAlB-type ceramics. The synthesis, microstructure, and properties of MoAlB samples will be discussed in next sections. The first work by Okada [6] discussed single crystal structure and characterizations of the ternary borides TMAlB (TM=Mo,W) in 1998. The MoAlB ceramic becomes a popular material to study recently because of its oxidation resistance at high temperature. Thus, more mechanical, electrical, thermal, and material properties are studied. For example, Kota *et al*. [7] found polycrystals of MoAlB stable at least 1400 ℃ in 2016.

Therefore, the MoAlB is a high temperature resistant ceramic with great promise. The motivation of this project is using an efficient method to fabricate the MoAlB samples with high purity.

1.2 Crystal Structure

Crystal structures of the MoAlB were proposed by Jeitschko [8]. Then researchers used chemical analysis and precise instruments to prove its unit cell and nanolaminated structure.

1.2.1 Orthorhombic crystal

Rieger *et al*. [9] reported MoAlB phase was orthorhombic, and its group space was Cmcm in 1961. The orthorhombic crystal is rectangle prism with a three-dimensional coordinate a, b, and c in Figure 1.1. The length a, width b, and height c of the rectangle prism are not equal.

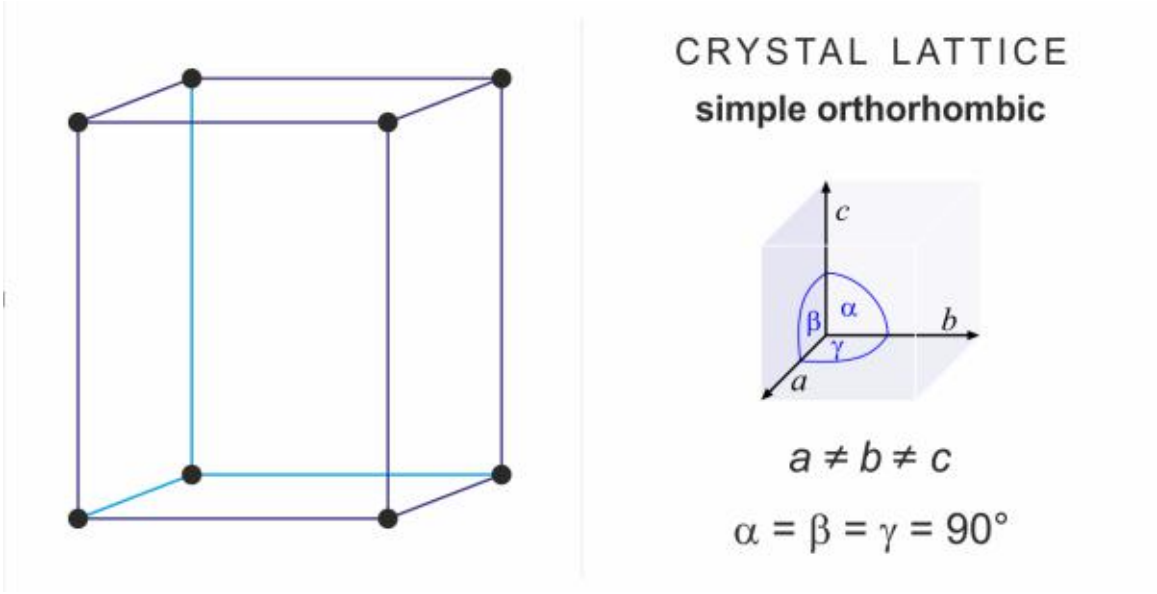

Figure 1.1: Simple orthorhombic crystal [10]

The MoAlB crystallized with an orthorhombic unit cell having the lattice constants a = 0.3212 nm, b = 1.3985 nm, c = 0.3102 nm, and V = 0.1393 nm^3 was reported by Jeitschko [8] in 1966. Besides, the MoAlB crystal structure shown in Figure 1.2 was determined by using single crystal structure film technique [8].

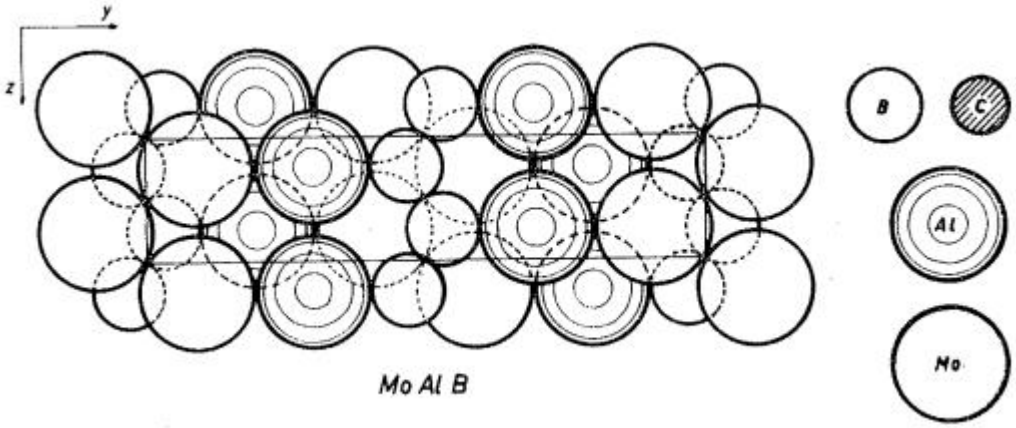

Figure 1.2: Crystal structure of MoAlB determined by Jeitschko [8]

1.2.2 Description of the MoAlB crystal structure

The MoAlB unit cell of three dimensional model is illustrated in Figure 1.3, which is reserved by the software PDF-4+2016 (2016 international center for diffraction data). The crystal structure shows that three elements Mo, Al and B are stacking in sequence in a unit cell. Aluminum atoms (Gray balls) are sandwiched between molybdenum (Green balls) and boron atoms (Pink balls). The b axis is much longer than the a and the c axis. It is bipyramid structure which is one of orthorhombic unit cells.

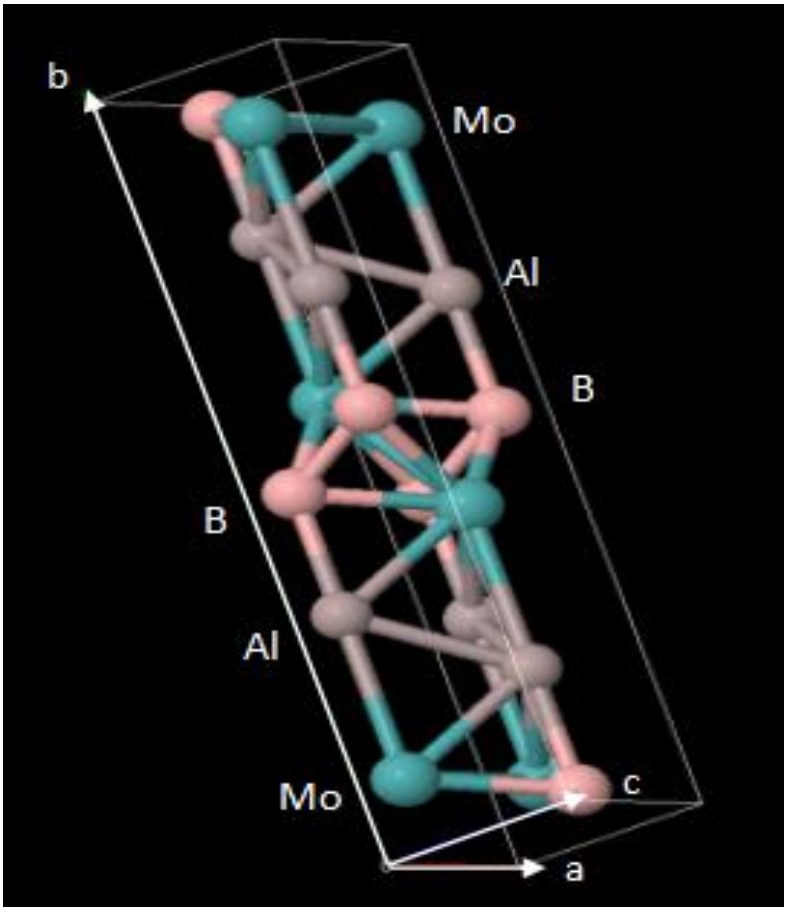

Figure 1.3: MoAlB unit cell (Pink ball is B atom, green ball is Mo atom, and gray ball is Al atom)

The MoAlB crystal structures are shown in Figure 1.4 [6] and Figure 1.5 (PDF-4+2016). Both figures are illustrating the a-plane which is along the b and the c axis, and the unit cells are outlined as rectangles (b and c sides) in both figures. The Figure 1.4 is an ichnography and the Figure 1.5 is a stereogram.

The structures demonstrate a triangular prismatic array of six molybdenum atoms surrounding each boron atom, one aluminum and two boron atoms situated outside the rectangular faces of the triangular prism, and aluminum atoms forming folded metal layers and interleaved between the molybdenum double layers [6]. All prism axes are parallel to the b axis, and the boron atoms form the B-B zigzag chains in the c axis [6].

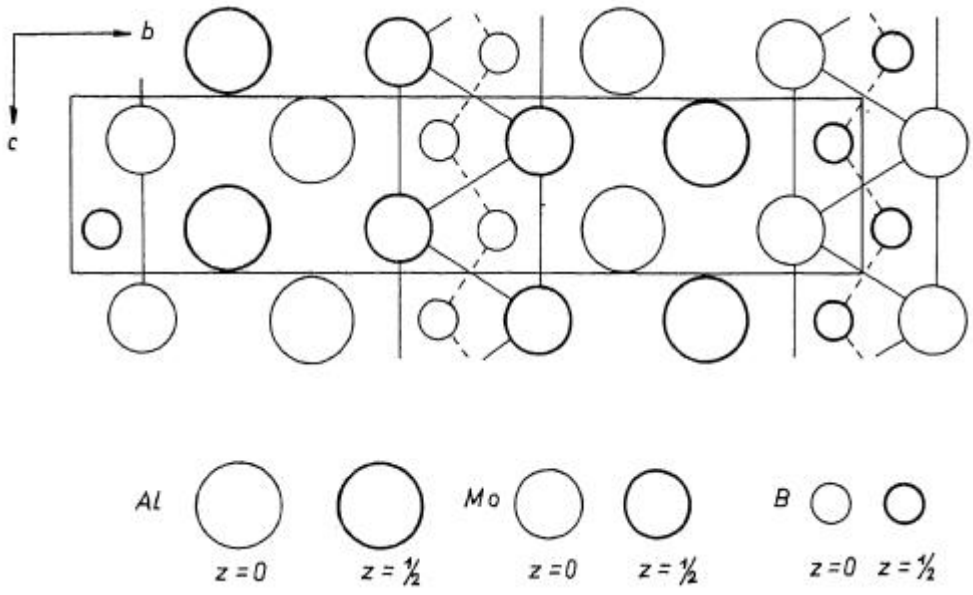

Figure 1.4: Ichnography of MoAlB crystal structure in the a-plane along b and c axis [6]

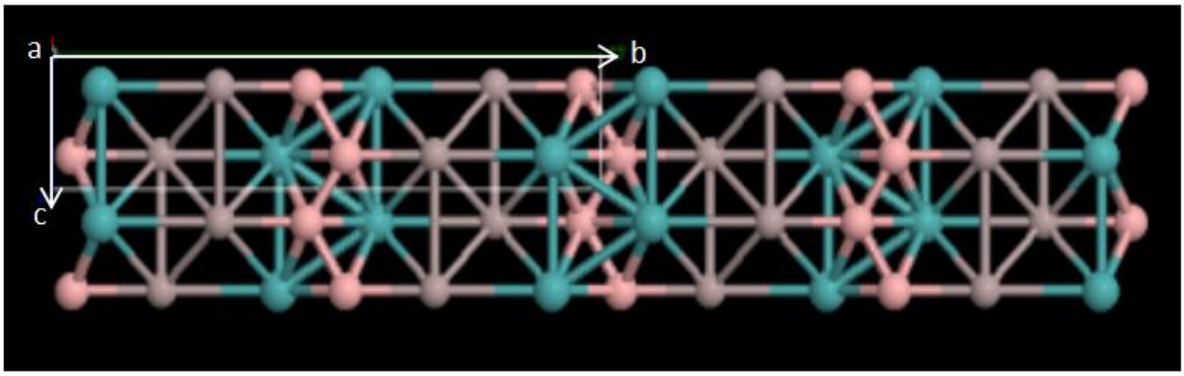

Figure 1.5: Stereogram of MoAlB crystal structure in the a-plane along b and c axis (Pink ball is B atom, green ball is Mo atom, and gray ball is Al atom)

1.3 Synthesis of the MoAlB ceramics

Single crystals and polycrystals of MoAlB are synthesized in different methods, but synthesis condition should be in high temperature environment. The single crystal means that atoms are periodic arrangements in the entire volume, which is shown in Figure 1.6 (a). The polycrystal shown in Figure 1.6 (b) has multiple grains which are formed by small single crystals. The polycrysta has grain boundaries.

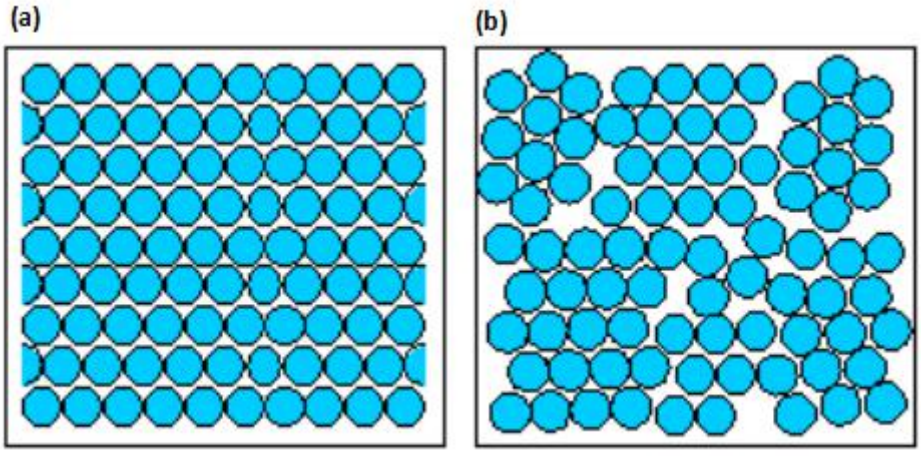

Figure 1.6: (a) Single crystal periodic arrangements; (b) Polycrystal hasing multiple grains [11].

The synthesis of large single crystals was first reported by Okada [6]. They fabricated with the method of high-temperature crystal growth [6]. One of methods synthesizing polycrystals of MoAlB is using hot pressing method by Kota *et al* [7]. The sample of polycrystal is a bulk form with a cylindrical prism after fabricating. Besides, an innovative method spark plasma sintering (SPS) was applied in fabricating polycrystals of MoAlB. The SPS is an important part for this thesis, and detailed information about synthesis will be introduced in Chapters 2 and 3.

1.3.1 Single crystals by crystal growth method

Synthesis of the MoAlB single crystals is by the method of crystal growth at the high temperature environment. Pure molybdenum (Mo) powders, boron (B) powders, and aluminum (Al) chips were mixed in a molar ratio of 1.0 : 1.0 : 53.3, respectively [6]. The mixtures were placed in alumina crucible and heated in argon atmosphere at 1500 ℃ for 10 hours [6]. When it cooled down to the room temperature, the sample was placed in hydrochloric acid (6 mol/L) for 7 days to dissolving excess aluminum [6]. The largest single crystal of MoAlB sample with dimension 1.0 × 1.0 × 5.1 mm^3 was selected under an optical microscope [6].

1.3.2 Hot pressing method

The method of synthesis of the MoAlB polycrystals was using the hot pressing. Pure molybdenum boride (MoB) and aluminum (Al) powders were mixed homogeneously in a molar ratio of 1.0 : 1.3 [7]. The mixtures were placed in a graphite foil lined cylindrical graphite die and heated at 1200 ℃ for 5.8 hours with

pressure 39 MPa [7]. After cooling to the room temperature, the MoAlB polycrystals with a bulk form were obtained.

1.3.3 Spark plasma sintering

The spark plasma sintering (SPS) is a new technology of powder metallurgy sintering which is sintering powders in a graphite die by electric discharging with a high pressure and vacuum environment. The heat is generated by pulsed direct current producing the spark plasma between powders, and the high pressure is caused by the hydraulic power compressing punches. The process of sintering illustrates that powders are compacted and formed a solid mass of material by heat and pressure. Atoms in the material diffuse across the boundaries of the particles, and the particles are fused together to create a solid mass because of an attraction between atoms in the high temperature and pressure environment. The spark plasma creates the environment of sintering. The powders finally are formed a fully dense bulk after electrical discharge activation, thermoplastic deformation and cooling down to the room temperature.

The SPS configuration in Figure 1.7 reveals that the control system commands whole system operating. The vacuum pump and inert gas control operating environment with vacuum, air and argon gas in the chamber. The hydraulic power provides pressure to compress punches, and the pulsed direct current power produces electrical discharge on the electrodes. The direct current is going through the powders in the mold when the powders are activated by the electrical discharge. The thermal

couple and optical pyrometers can measure the temperature in the mold, and the cooling system can provide cooling water to cool the temperature in the chamber. Transmit programs to the control system, and it can control temperature, pressure and time to fabricate samples by commanding these subsystems.

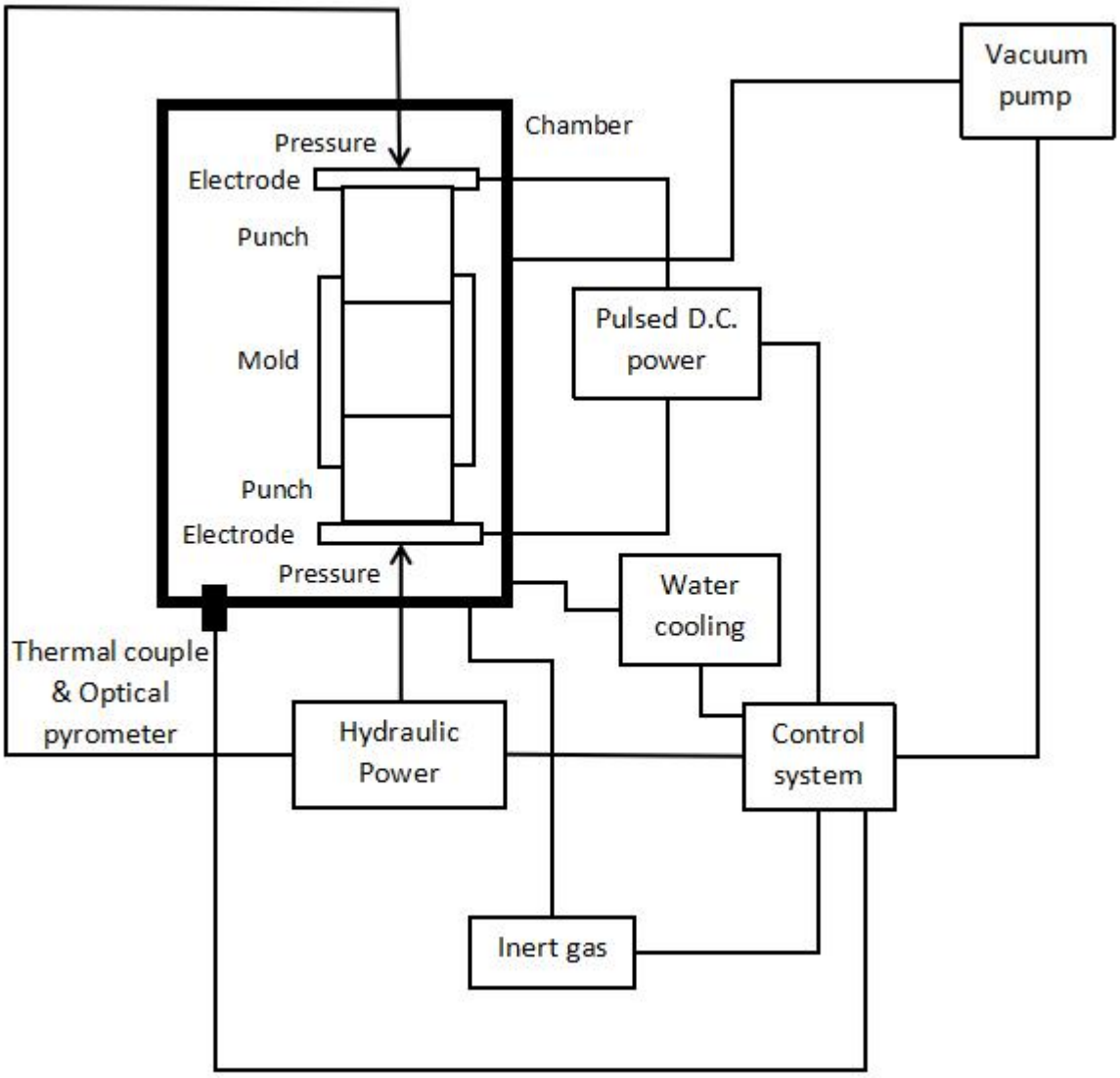

Figure 1.7: Configuration of the SPS

Using the method of the SPS to fabricate the MoAlB polycrystal is referred by the hot pressing method. The biggest advantage of the SPS is spending very short time to synthesize the MoAlB samples with high purity. For example, the SPS method spends

about 1 h to fabricate a bulk sample with a high purity (> 98 vol. %) and a high relative density (> 97 %) at the temperature 1200 ℃ and pressure 100 MPa for 8 min.

1.3.4 Comparison of different methods

The different methods of synthesizing MoAlB crystals have close heating temperatures (1200-1500 ℃), but they have large differences in fabricating time and pressure. The MoAlB single crystals fabricated by crystal growth method need long time 10 hours and free space to grow, but polycrystals synthesized by the hot pressing and the SPS methods need high pressure and less time of 5.8 and 1 hours, respectively. That is the reason why different fabricating methods obtain monocrystals and polycrystals separately. Besides, dimensions of samples are different by using different methods. The dimension of single crystal is small, which should be selected under the optical microscope, but the shape of polycrystals is bulk form with cylindrical prism.

Table 1.2 lists three methods which are the crystal growth, the hot pressing, and the spark plasma sintering to fabricate the MoAlB samples with different synthesis conditions. The SPS has a high efficiency to fabricate pure MoAlB samples compared with other methods.

	Obtained crystal	Temperature (℃)	Pressure (MPa)	Time (hour)
Crystal growth method	Single crystal	1500	0.101 (Normal atmosphere)	10
Hot pressing	Polycrystal	1200	39	5.8
Spark plasma sintering	Polycrystal	1200	100	1

Table 1.2: Different methods of fabricating the MoAlB samples with different synthesis conditions

1.4 Microstructure of MoAlB crystals

The crystal structure of MoAlB is mentioned above. Its microstructure is confirmed by using X-ray diffraction (XRD), scanning electron microscopy (SEM), High-resolution scanning transmission electron microscopy (HRSTEM), and some chemical analysis.

1.4.1 Microstructure of MoAlB single crystals

The MoAlB single crystals have silver color and metallic luster reported by Okada [6]. Besides, the b-plane of a needle-like rectangular of the single crystal can be observed by the SEM in Figure 1.8 [6]. The Figure 1.8 shows the b-plane is extending in the direction of the c axis. The unit cell parameters (a = 0.3213 nm, b = 1.3986 nm,

and c = 0.3195 nm) are close to the Jeitschko's results (a = 0.3212 nm, b = 1.3985 nm, and c = 0.3102 nm) [6, 8]. The results of chemical analysis show Mo, Al, and B elements in a molar ratio of 1.09 : 1.04 : 1.00, which is close to theoretical molar ratio (Mo : Al : B = 1 : 1 : 1) [6].

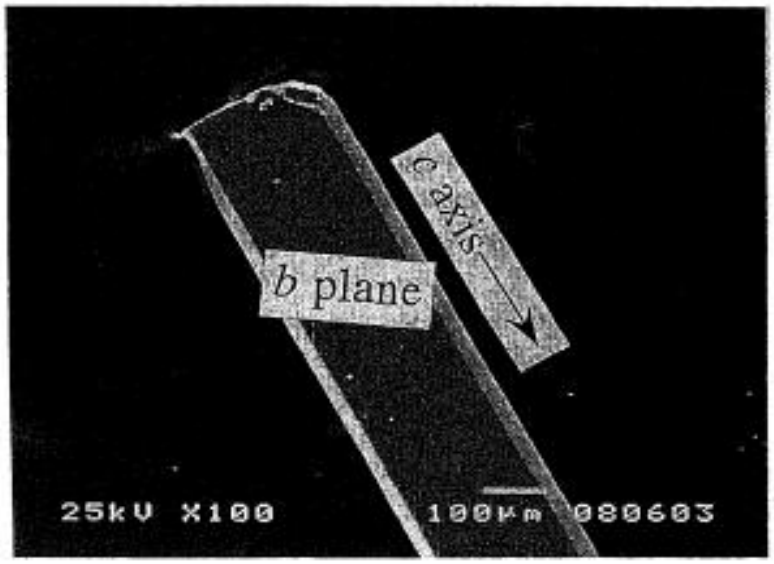

Figure 1.8: SEM photograph of single crystal MoAlB [6]

1.4.2 Microstructure of MoAlB polycrystals

Figure 1.9 reveals that the X-ray diffractograms of MoAlB polycrystal in top surface and cross-section; besides, they are comparing with calculated diffractogram (Standard diffraction pattern) [7, 12]. Intensity ratios of sample's top face are different from the standard diffraction pattern. Higher intensity of the {0k0} peaks of the top surface is attributed to the hot pressing which helps orient the {010} axis of the grains parallel with the hot pressing direction preferentially [7]. Besides, there are weak peaks at 22.8° and 43.9° of the top surface in the Figure 1.9 [7]. These peaks belong

to Al_3Mo and impurities. After the Rietveld refinement on cross-section, the results show that MoAlB phase is major and Al_3Mo phase is 3 vol. %; besides, the lattice constants of a = 0.321 nm, b = 1.398 nm, and c = 0.310 nm are agreeing with the results of Jeitschko [7, 8].

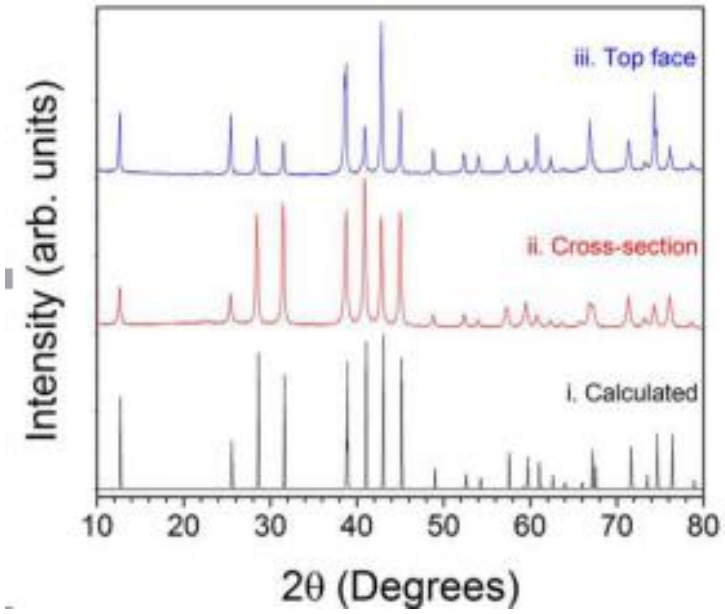

Figure 1.9: X-ray diffractograms of top face, cross-section, and standard pattern [7]

The image of High-resolution scanning transmission electron microscopy (HRSTEM) in the [100] zone axis shows the evidence of nanolaminated structure consisting of Mo-B layers with alternating Al layers in Figure 1.10 (a). Right inset of the Figure 1.10 (a) shows selected area electron diffraction (SAED) pattern along the [100] zone axis, and left inset illustrates the positions of Mo, Al, and B atoms in the crystal structures [7]. The SEAD along the [100] zone axis also confirms the orthorhombic symmetry of MoAlB with its special structure in Figure 1.10 (b) [7].

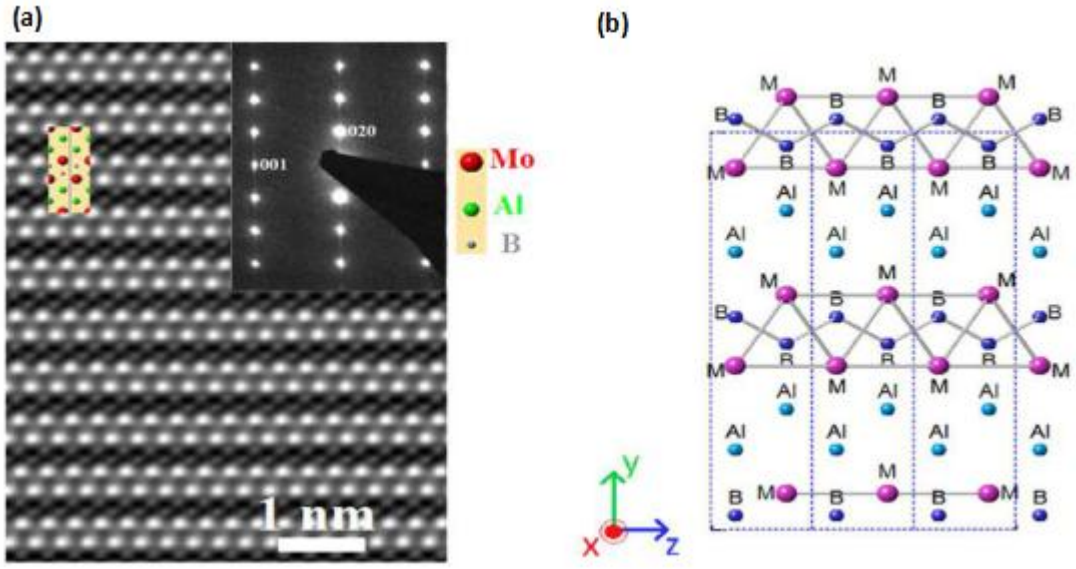

Figure 1.10: (a) HRSTEM image of MoAlB along the [100] zone axis. Right inset shows the SAED pattern and left insert shows Mo, Al, and B atoms in the crystal structures; (b) MoAlB crystal structure on the (100) plane [7].

Secondary electron micrographs of the SEM show the cross-sectional fracture surface at low and high magnification in Figure 1.11 (b) and (c) [7]. The micrographs reveal striations and layered structure of grains. The striations are the characteristic of nanolaminated materials [7].

Backscattered electron micrograph of the SEM in Figure 1.11 (a) shows major phase of white regions, minor phase of gray regions, and minor phase of dark regions. The EDS shows that the gray phase is an aluminum-molybdenum impurity with a molar ratio of 2.5 : 1, so it is determined as Al_3Mo [7]. The Al_3Mo phase is about 6 ± 2 vol. % in this image. In addition, the dark phase is Al_2O_3 about 3 ± 0.5 vol. % [7]. The impurities of the MoAlB sample will be discussed in Chapter 3 by comparing the results of the MoAlB samples fabricated by the SPS method.

The purity of the MoAlB polycrystals synthesized by the hot pressing method is about 94 vol. % measured by the backscattered electron micrograph. The volume percentage of the impurities Al_3Mo and Al_2O_3 is low, so the mechanical and electrical properties will not be influenced.

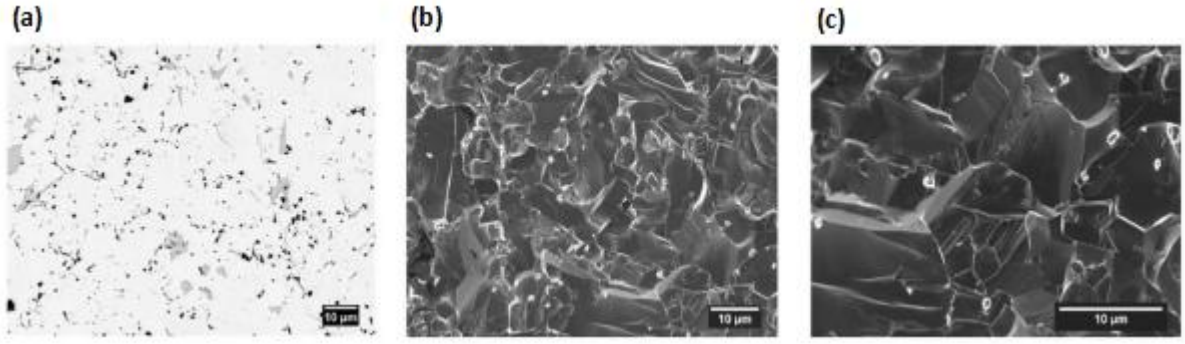

Figure 1.11: (a) Backscattered electron micrograph of MoAlB on cross-section; (b, c) Secondary electron micrographs of the cross-sectional fracture surface at low and high magnification [7].

1.5 Mechanical properties

Mechanical properties of the MoAlB include hardness, strength, fracture toughness, elastic modulus, etc. The Vickers hardness is applied in measuring ceramic's hardness commonly. More information about the Vickers hardness will be introduced in Chapter 2 and 3. In addition, the ultimate compressive strength is used to measure MoAlB samples' strength. Ceramic materials have high values of the Vickers hardness and the ultimate compressive strength, but they have low values of the tensile strength.

The Vickers hardness measured on the b-planes of single crystal MoAlB is in the range of 10.3 ± 0.2 GPa by Okada [13]. The hardness of polycrystal on the

cross-section is approximately constant at 10.6 ± 0.3 GPa at different loads from 1kgf to 10 kgf by Kota *et al*. [7]. These two results of the Vickers hardness values are close. The Vickers hardness results of MoAlB samples are moderately lower, which are comparing to its binary transition metal borides such as MoB (H_v = 23 GPa,) [14], MoB_2 (H_v = 21 - 27 GPa) [5, 15] . The ternary transition metal boride MoAlB is a bit softer than its binary counterparts because of the Mo-Al bonds formed in the ternary transition metal boride. The Mo-Al bond is the metallic bond which is weaker than covalent bond (B-B) and ionic bond (Mo-B).

The SEM micrograph in Figure 1.12 (a) shows an indentation of the Vickers hardness formed under 9.8 N load [7], and there is no crack along the edge of this indentation. The nanolaminated structure in the MoAlB sample can decrease the formation of cracks when this sample is indented. Figure 1.12 (b) reveals the Vickers hardness indentation of zirconium diboride (ZrB_2) which has dominate cracks along the edge of the indentation [16]. Thus, it confirms the MoAlB ceramics have a unique property of mechanical damage tolerance because of the nanolaminated structure consisting of Mo-B layers with alternating Al layers.

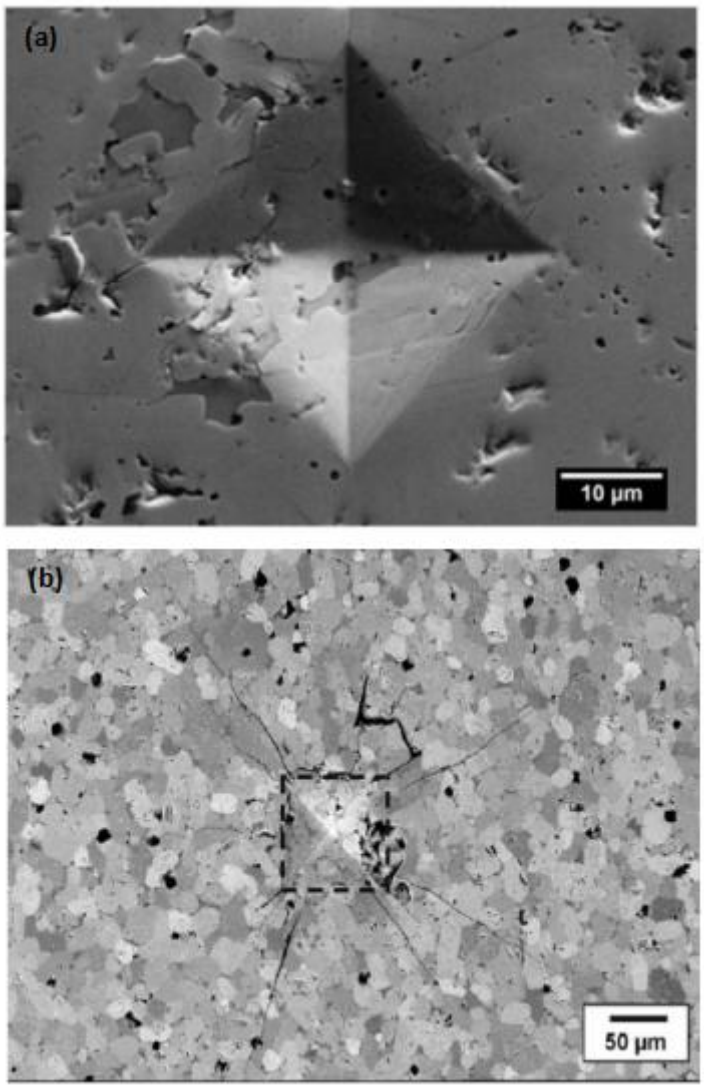

Figure 1.12: (a) A SEM micrograph of the Vickers hardness indentation of MoAlB, (b) A SEM micrograph of the Vickers hardness indentation of ZrB_2 [7] [16].

The ultimate compressive strength is 1940 ± 103 MPa in the room temperature by Kota *et al*. [7]. The high value of compressive strength agrees well with the property of ceramics.

1.6 Electrical resistivity

The electrical resistivity (ρ) of the MoAlB sample is increasing linearly with temperature above 100 K, and the resistivity of its polycrystal is 0.36 μΩm at the

temperature 300 K by Kota *et al*. [7]. It is closed to the electrical resistivity of metal. For example, the resistivity of pure molybdenum metal is 0.055 μΩm at 300 K [17]. Single crystals of MoAlB have a higher value of resistivity 0.64 μΩm which was measured along the b-plane reported by Okada *et al* [13].

The electrical resistivity of MoAlB polycrystal should be higher than single crystal theoretically because the polycrystal has more grain boundaries which like barriers decreasing electrical conductivity. However, the results are in contrast because a few impurities in the MoAlB samples influence the electrical resistivity. For example, the impurity Al_3Mo in the MoAlB polycrystals can increase the sample's electrical conductivity. That is the reason why the polycrystal's electrical resistivity is lower than single crystal's.

1.7 Oxidation resistance at high temperature

Oxidation of MoAlB at high temperature is caused by the oxidizing reaction between inward diffusion of oxygen ions and outward diffusion of molybdenum and aluminum ions [18]. At a specific temperature, the MoAlB sample surface can form an adherent alumina scale which can protect the MoAlB sample from oxidation at high temperature. The oxide layer can keep the MoAlB sample from corrosion at high temperature because the alumina layer like a shield can prohibit the inward diffusion of oxygen ions. The alumina layer has properties of denseness and slow growth; besides, it has low diffusion of O, Mo, and Al ions. That is the reason why this kind of ceramic materials can be resistant to oxidation damage. However, oxygen can ingress

sample's body rapidly and lead to heavy oxidation after the protective layer cracks at higher temperature [18].

Okada did preliminary study revealing the oxidation reaction of single crystal beginning at 740 ℃ [6]. Besides, the final oxidation products contain MoO_3, $Al_5(BO_3)O_6$, and $Al_8B_4O_{33}$, respectively [6]. The alumina of MoAlB samples formed at temperature 740 ℃, and they can be oxidized below temperature 1200 ℃.

Kota *et al*. analyzed polycrystal MoAlB bulks oxidation at the constant temperature 1100, 1300, and 1400 ℃ [7]. The graph of Figure 1.13 shows the oxidation for 100 h at 1100 ℃ formed 3 ± 0.4 μm thick scale of Al_2O_3 and the oxidation for 200 h at 1300 ℃ formed thick scale of Al_2O_3 and MoB [7]. The inset in the Figure 1.13 shows the SEM micrograph of the layers of MoAlB and Al_2O_3 of the cross section at 1300 ℃ after 200 h [7]. It means the MoAlB sample can be resistant to oxidize at temperature 1300 ℃.

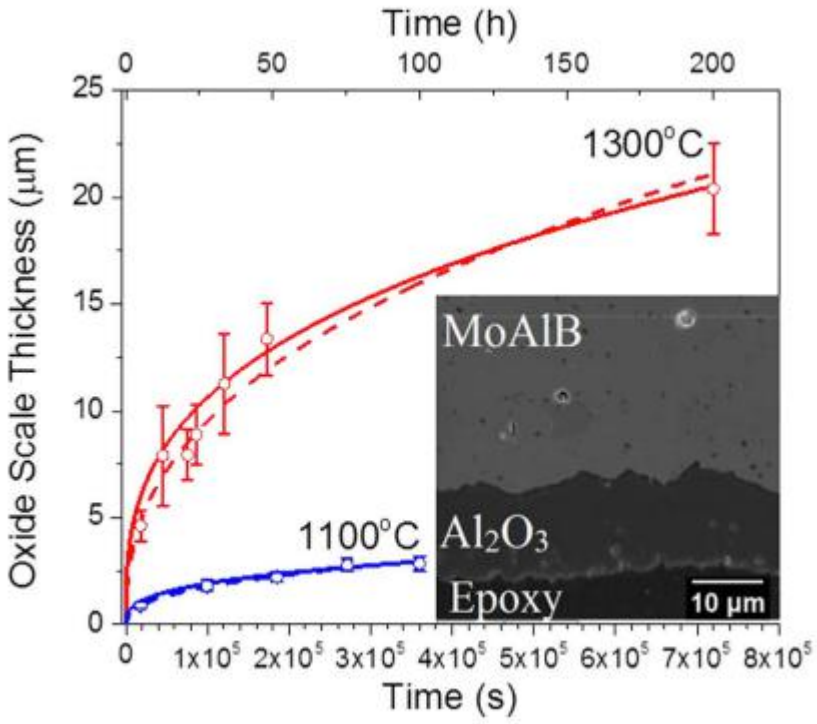

Figure 1.13: Blue line is the oxidation for 100 h at 1100 ℃, and the red line is the oxidation for 200 h at 1300 ℃; Inset is the SEM micrograph of the cross section for 200 h at 1300 ℃ [7].

The samples at temperature 1400 ℃ for 10 h and at 200 h at 1300 ℃ were analyzed by the XRD in Figure 1.4 [7]. Dominant phase of the sample at 1400 ℃ after 10 h is Al_2O_3, and few phases are MoAlB and MoB. In addition, dominant phase of the sample at 1300 ℃ after 200 h is MoAlB, and few phases are MoB and unknown compositions.

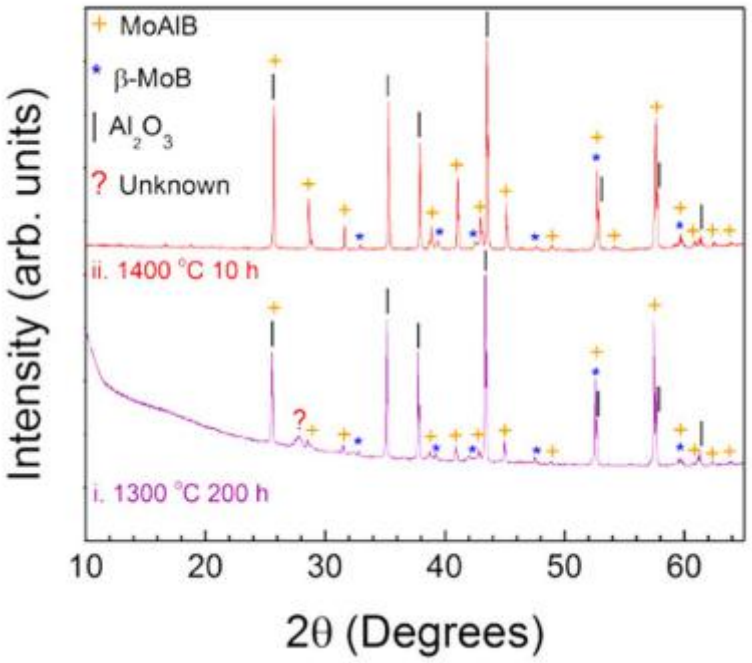

Figure 1.14: XRD results of samples at temperature 1400 ℃ for 10 h and at 200 h at 1300 ℃ [7]

Chapter 2: Experimental Procedure

2.1 Synthesis of MoAlB

The synthesis of MoAlB ceramics is used to the method of spark plasma sintering (SPS). Mixtures of molybdenum boride (MoB) and aluminum (Al) powders are sintered in a graphite mold with high temperature and high pressure condition. The final product of chemical reaction is MoAlB a cylindrical bulk. The chemical equation shows

$$MoB + Al \rightarrow MoAlB, \ (1100\ ℃ < T < 1200\ ℃). \qquad (2\text{-}1)$$

The chemical equation is a combination reaction, and an atomic ratio of MoB to Al to MoAlB is 1 : 1 : 1 theoretically. The SPS system can provide good reaction condition with high temperature and high pressure. Eventually, optimized reaction condition should be determined from the purity of product MoAlB.

2.1.1 Preparation for synthesizing

Raw materials were chosen from powders MoB (99%, < 38 μm, Alfa Aesar, Ward Hill, MA, USA) and powders Al (-325 mesh, 99.5%, Alfa Aesar, Ward Hill, MA, USA). The MoB and Al powders were mixed in an atomic ratio of 1:1.1 with 12 grinding balls (3/8 inch diameter, tungsten carbide, OPS Diagnostics LLC, Lebanon, NJ, USA) and ethanol (>99.7% pure) in a plastic bottle. The volume of ethanol should submerge the mixtures in a plastic bottle. All procedures of mixing were completed in a glove box under argon atmosphere to avoid oxidation.

The mixtures in the bottle were rotated for 24 hours on the tube roller (Scilogex MX-T6-S, SoCal BioMed, Newport Beach, CA, USA) which is shown in Figure 2.1 (a). The powders can be milled homogeneously by 24 hours rotation with grinding balls. The process of ball milling can decrease the powder's size. Then the plastic bottle containing ball-milled powders was dried in a tube furnace (MTI GSL-1700X-S60HG, MTI, Richmond, CA, USA) in Figure 2.1 (b), which was setting temperature at 70 ℃ for 5 hours with ventilating argon. After drying, the ethanol in the bottle were volatilized completely. Finally, the grinding balls were taken out in the glove box under argon atmosphere. The ball-milled powders left in the plastic bottle were used to fabricate the MoAlB samples by using the SPS method.

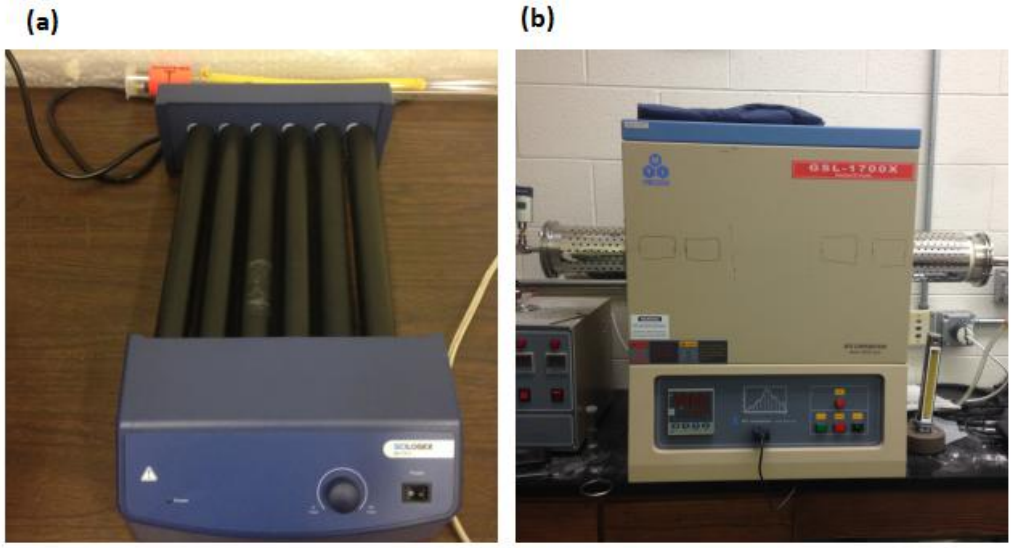

Figure 2.1: (a) Tube roller, (b) Tube furnace

2.1.2 Spark plasma sintering

The MoAlB samples were synthesized and simultaneously sintered by using the

SPS system (Model 10-4, Thermal Technology LLC, Santa Rosa, CA, USA) in Figure 2.2. The mixture powders were placed in the graphite die. The SPS could provide uniaxial pressure and high pulsed current to compress and heat the powders. Eventually, a bulk sample MoAlB can be formed in several minutes.

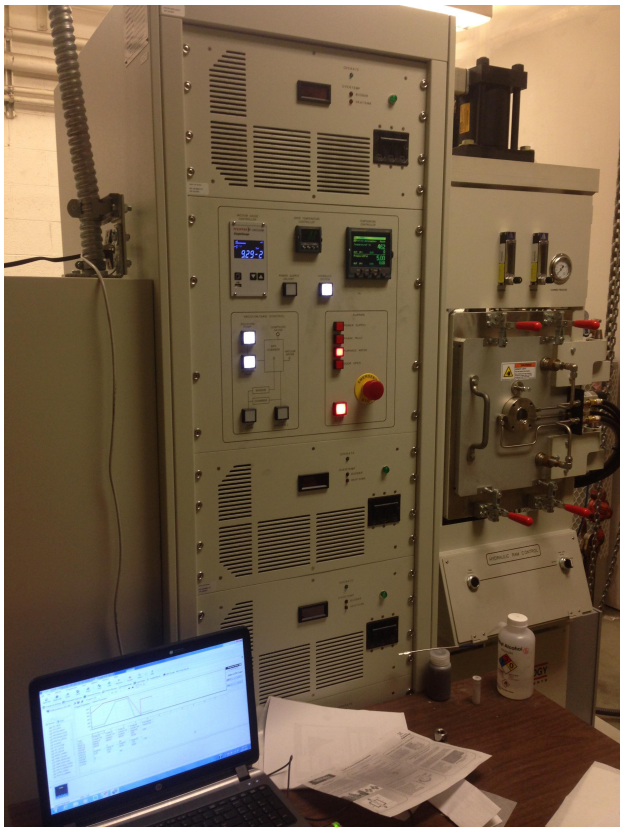

Figure 2.2: System of spark plasma sintering

The mixture powders were encased by graphite papers in a cylindrical graphite mold which is in the chamber of the SPS machine. The initial pressure of the chamber was set as 20MPa after vacuuming three times, and the temperature was set at 24 ℃ for room temperature. The mixture powders were heated at the rate of 100 ℃/min and pressurized by 40 MPa/min. Then mixtures were sintered in a temperature region between 1100 and 1200 ℃, and they were also compressed in a pressure region

between 50 and 100 MPa. Both high temperature and pressure condition was processed in 8 minutes for sintering. Finally, the temperature and pressure of chamber should be decreased to 24 ℃ and 5 MPa by the rate of -100 ℃/min and -30 MPa/min, respectively.

More specifically, Table 2.1 lists the detailed program of fabricating the MoAlB sample in a synthesis condition with temperature 1100 ℃ and pressure 50 MPa. The initial condition was set, and the temperature was increased to 600 ℃with rate 100 ℃/min, which is a middle temperature. After keeping temperature 600 ℃ for 10 s, peak temperature 1100 ℃ was reached by same heating rate. Then the pressure in the chamber began to compress with compressing rate of 40 MPa/min, and maximum pressure 50 MPa was achieved quickly. Sintering time was set 8 min in this synthesis condition. Finally, the temperature and pressure was decreased to final condition simultaneously.

	Temperature (℃)	Heating Rate (℃ /min)	Pressure (MPa)	Compressing Rate (MPa/min)	Time (min)
Initial Condition	24	0	20	0	0
Increase Temperature & Keep Pressure	600	100	20	0	5.76
Keep Temperature & Keep Pressure	600	0	20	0	0.17
Increase Temperature & Keep Pressure	1100	100	20	0	5
Keep Temperature & Increase Pressure	1100	0	50	40	0.75
Keep Temperature & Keep Pressure	1100	0	50	0	8
Decrease Temperature & Decrease Pressure	24	-100	5	-30	30
Final Condition	24	0	5	0	0

Table 2.1: Process of synthesizing a MoAlB sample with temperature 1100 ℃ and pressure 50 MPa for 8 minutes

Fabricating a MoAlB sample takes about 1 hour, and most time of synthesis is spent in cooling chamber by the cooling water. Comparing with the hot pressing method, high efficiency of synthesizing the MoAlB crystal is a big advantage of the SPS method.

2.2 Microstructure and properties analysis of MoAlB samples

The microstructures and chemical compositions of MoAlB samples were characterized by some instruments. X-ray diffraction (XRD) diffractometer and energy dispersive X-ray spectrometry (EDS) of scanning electron microscopy (SEM) are used to analyze elemental compositions in a sample including impurities' compositions. Besides, the SEM can scan micrographs by secondary electrons and backscattered electrons. The secondary electron micrographs can describe topography of sample surface in micro-level. The backscattered electron micrographs can reveal different color and shape of phases on the sample surface. Therefore, the purity of sample should be calculated.

The property of MoAlB sample includes physical property density, mechanical property Vickers hardness, and property of oxidation resistance. The density was measured by a density balance device which is followed by the Archimedes principle. The Vickers hardness was measured by a special indentation and calculated by a specific formula. The Oxidization resistance was measured at temperature 1400 ℃, and the elemental compositions of a sample were analyzed by the XRD and SEM after oxidation test.

2.2.1 Sample preparation

The MoAlB samples were removed from the chamber of the SPS system after finishing sintering. The shape of each sample was a cylindrical bulk which its diameter was about 20 mm respectively in Figure 2.3. Besides, each sample' surface was covered by a graphite layer formed after the SPS. The graphite layers should be eliminated before microstructure and properties analysis.

Figure 2.3: The sample surfaces covered with graphite layers

Top and bottom faces of each sample were ground by abrasive papers with 240 grit to grind the graphite layer off. Then the grinding papers in order of 400, 600, 800, and 1200 grit were used to grind the sample surface. Afterwards, the top surface was polished by alumina powders (0.3 μm diameter). The top face should be kept flat, and there was no obvious scratch on the top surface after polish. Acetone (>99.2% pure) and alcohol (>99.7% pure) were used to rinse the top surface. After grinding process, thickness of samples was about 2 mm. A gap was knocked at each sample's edge in

order to observe fracture surface by the SEM. Figure 2.4 shows a sample with top surface and a gap after finishing sample preparations.

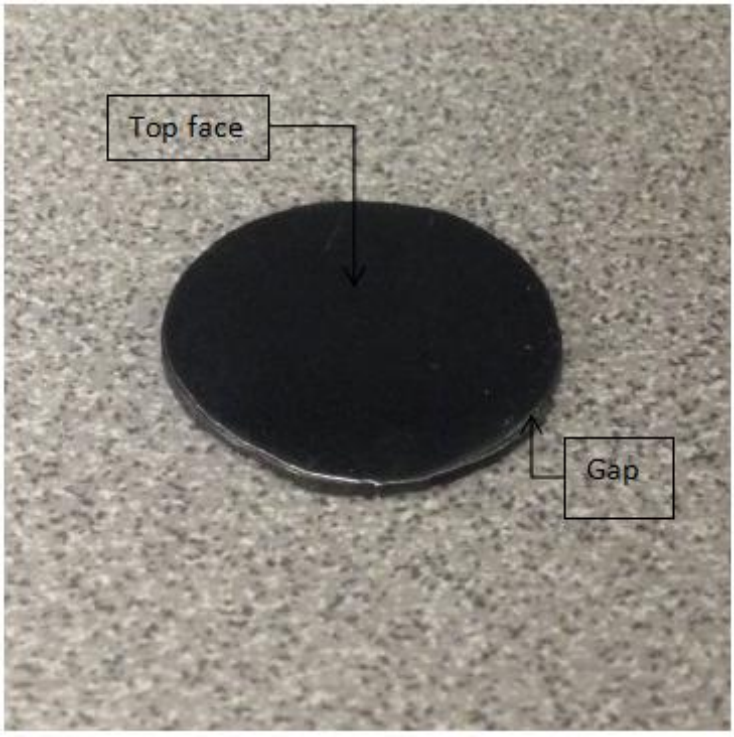

Figure 2.4: Top surface and gap in a sample after finishing sample preparations

2.2.2 Density measurement

A density balance kit (Density kit for XP/XS analytical balances, Mettler Toledo LLC, Columbus, OH) was applied in measuring each sample's density. Figure 2.5 illustrates the device which is made up of a low glass beaker containing water, an electronic scale for measuring the samples' weight in the air and water, three holders placing samples in the air, and a steel basket placing samples in the water.

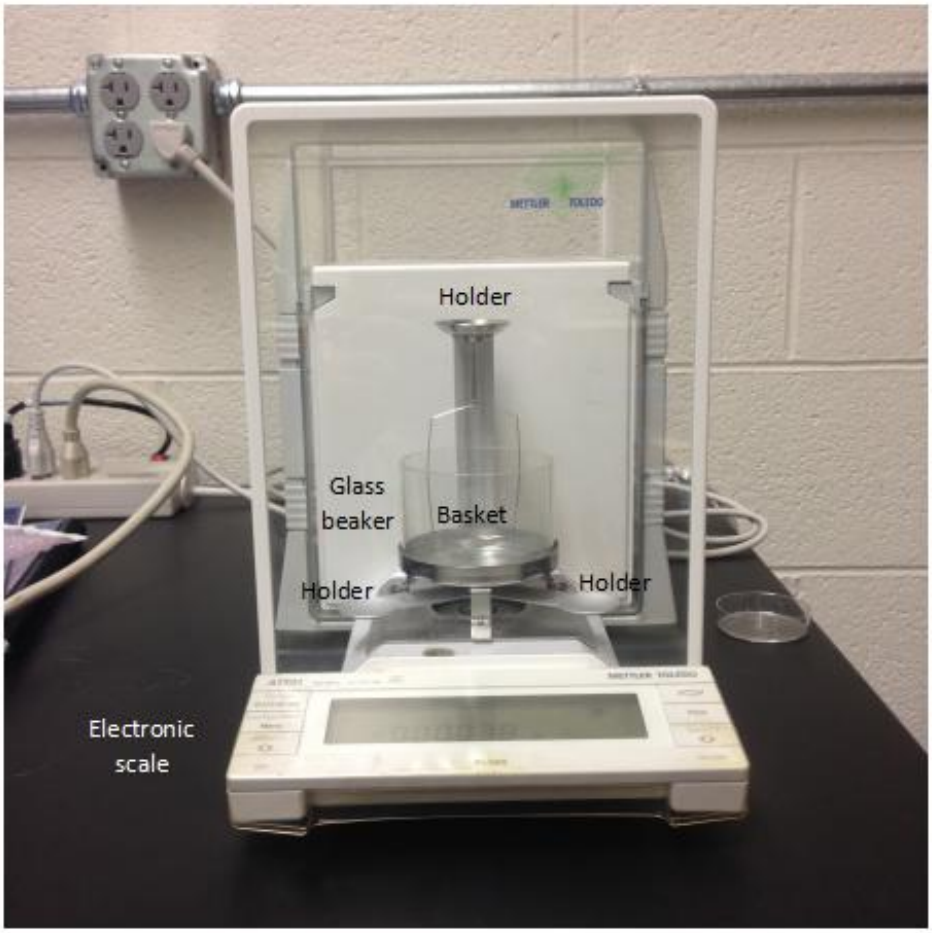

Figure 2.5: Density balance kit

Density of sample is determined by the Archimedes principle. A sample is immersed in the water, and it is buoyed up by a force which is equal to the weight of water that the sample displaces [19]. The water density ρ_w is known, and measure the samples' weights in the air (W_a) and water (W_w). Thus, sample's density (ρ) can be calculated by the following equation:

$$\rho = \frac{W_a \times \rho_w}{W_a - W_w} \tag{2-2}$$

Considering tiny influence of air buoyancy, above equation also can be rectified.

Density of air (ρ_a) is around 0.0012g/cm^3 in standard atmospheric pressure and temperature 20 ℃ [20]. The formula is written as follows:

$$\rho = \frac{W_a \times (\rho_W - \rho_a)}{W_a - W_W} + \rho_a \quad (2\text{-}3)$$

The water temperature measured was 23.2 ℃, and the density of water ρ_w determined was 0.99752 g/cm^3 by the density table for distilled water [20]. Each MoAlB sample was placed on the holder for measuring its weight in the air and placed on the basket for measuring weight in the water. Keep the water immersing total volume of each sample when weighing every sample in the basket. Two weights of every sample were measured 5 times. Then density of each measurement was calculated by the Formula 2-3. Finally, the mean value of each sample's density was calculated.

2.2.3 X-ray diffraction characterization

The X-ray diffraction is an analytic technique applied in identification of crystalline phase. Thereby, it can analyze crystalline structure and chemical compositions. The mechanism of XRD is constructive interference of the X-rays and the crystal of sample. An X-ray tube of the diffractometer produces CuK_α X-rays when a hot filament shoots high-power electron beam into a copper target. The X-rays have a constant wavelength, and the wavelength value is close to the spacing of atomic interface in the crystal of specimen. Thus, the crystal can be worked as raster for X-ray beam, and constructive interference will be produced.

The process of constructive interference is described by Bragg's law:

$$2d_{hkl}\sin(\theta) = n\lambda \tag{2-4}$$

where d_{hkl} is the spacing between two planes hkl, θ is the angle between the X-ray and the parallel plane, n is an integer, and λ is the wavelength of the X-ray. Figure 2.6 illustrates the Bragg's analysis for XRD by crystalline plane. The incident beams of X-ray radiates into crystalline planes, and 2 parallel beams (Beams 1 and 2) scatters in a specific direction. After scattering, they become two parallel diffracted beams (Beam 1' and 2'), and the distance of parallel beams are the atomic spacing through a range of 2θ angles. The atomic spacing converts to diffraction peaks in the X-ray diffractogram, so it can identify crystalline phase. The diffraction peaks are compared to the standard X-ray diffraction patterns (PDF cards) in order to identify compositions in the sample.

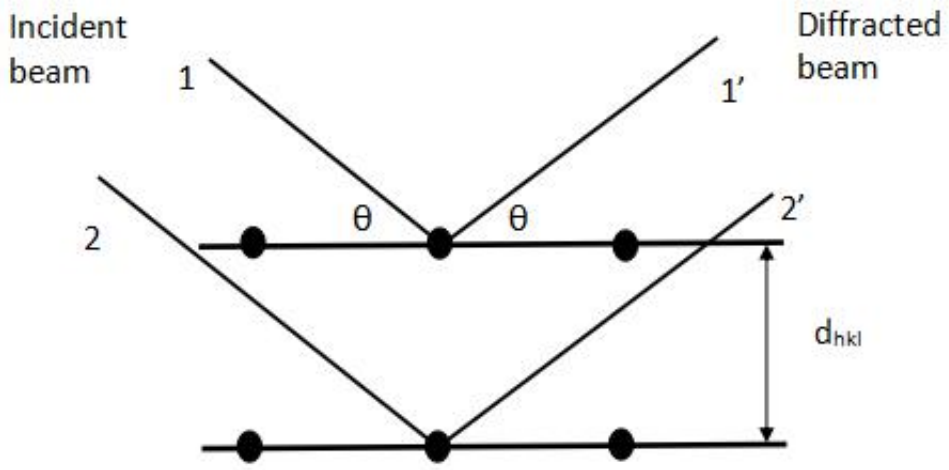

Figure 2.6: Bragg's analysis for XRD by crystalline plane

An X-ray diffractometer (PANalytical Empyrean Diffractometer, PANalytical, Westborough, MA, USA) was used for obtaining X-ray diffraction patterns of each MoAlB sample' top surface. The JADE software was applied in showing X-ray diffractogram of each sample. The compositions of each sample were analyzed by comparing to powder diffraction file (PDF) cards reserved by the software PDF-4+2016 (2016 international center for diffraction data).

2.2.4 Scanning electron microscopy

Scanning electron microscopy is a technique producing the images of specimen's microstructure by scanning with a focused beam of electrons. The specimen should be bulks or powders. The signals of imaging are from secondary electrons, backscattered electrons, and absorbed electrons. The electrons can produce signals containing information about sample's topography, morphology, composition, and crystalline structure after interacting with atoms of sample [21].

Figure 2.7 explains detailed mechanism of the SEM. The electron gun produces a beam of electrons with energy between 5 and 35 keV. The beam of electrons is focused by the first condenser lens and filtrated by the condenser aperture. Then repeat the process of condensation and constriction by the second condenser lens and objective aperture, respectively. At this time, the electron beam is formed in high intensity with s small beam diameter after two times of condensation and constriction. Afterwards, varying current in the scan coils can control electrons' direction and speed. Finally, the objective lens are used to condense the electron beam, and the

focused stream of electrons shoot to the sample surface. The detectors of the SEM are applied in receiving the signals produced by electrons interacting with atoms on the sample surface.

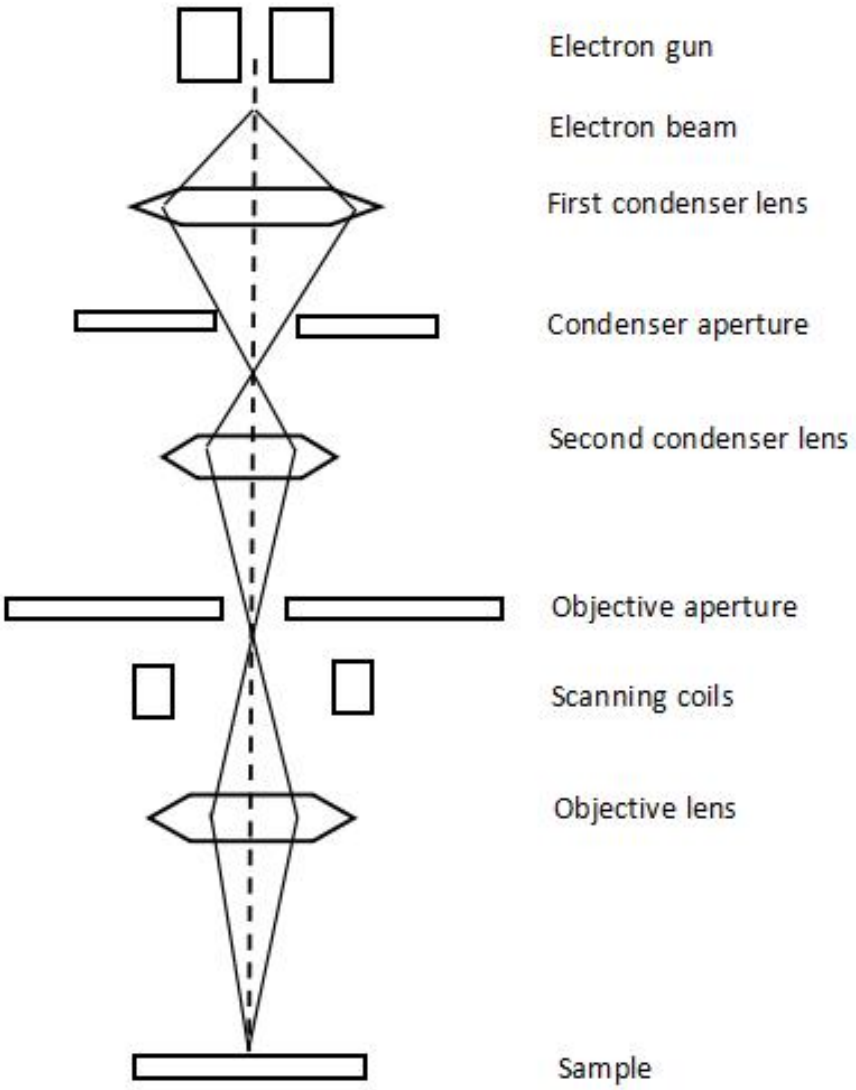

Figure 2.7: Mechanism of the SEM

The reaction of the beam of electrons and atoms on the sample surface can produce secondary electrons, backscattered electrons, characteristic X-rays, Auger electrons, absorbed electrons, and direct beam. The relationship of these products are shown in

Figure 2.8. The detectors detect them and convert to electric signals to image characterizing sample' microstructures. The secondary electrons are extranuclear electrons of sample's atoms ejected by the electron beam. They are from sample surface layer about 5 to 10 nm depth. The secondary electrons are sensitive to sample surface' topography, so they can show the topography information about the specimen's surface. The backscattered electrons from the incident beam are bounced back elastically by the sample's nucleus. They have the information about specimen's phase difference. Characteristic X-ray is produced by electrons of sample's atoms bombarded by high-energy electrons from the electron beam. The X-ray spectra can exhibit characteristic peaks identifying different elements in the region of the sample. The X-ray spectra is used for energy-dispersive spectrometry (EDS) analysis.

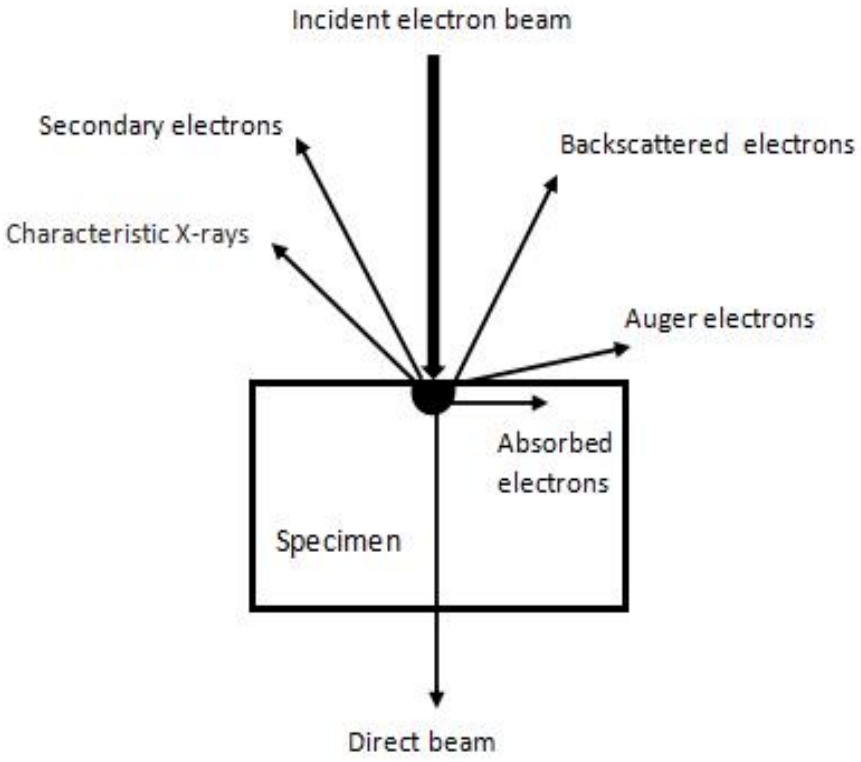

Figure 2.8: Different signals produced when incident electron beam reacting to specimen

The microstructure of each MoAlB sample was characterized by the SEM (FEI Nova NanoSEM 450, FEI, Hillsboro, OR, USA). The topographic micrographs of top surface and fracture surface were shown by secondary electrons. Then the backscattered electron micrographs were identified different phases on the top surface. The EDS was used to analyze elemental composition in each phase from the backscattered electron micrographs.

2.2.5 Vickers hardness

The Vickers hardness (HV) is a kind of hardness test with forming a square indentation. The shape of indenter is a pyramid cone, and the angle of opposite sides

is 136 degree. The material of indenter is diamond which has the highest hardness. The force of indenting is allowed between 1 to 100 kgf, and it applied on the sample's surface for a constant time about 10 to 20 s [22]. Figure 2.9 reveals the indenter impacting on the sample's surface by a constant load.

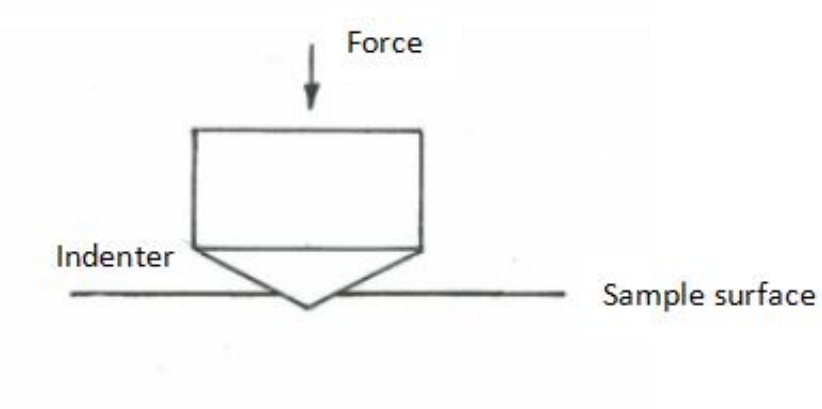

Figure 2.9: Vickers indenter impacting on the sample's surface

After indenting, an indentation are formed in the shape of a square with two diagonals shown in Figure 2.10. Use a microscopy to observe and measure the indentation of the Vickers Hardness. Measure the length of two diagonals in each indentation, and calculate its mean value. The length of diagonals are large, and the Vickers hardness value is small.

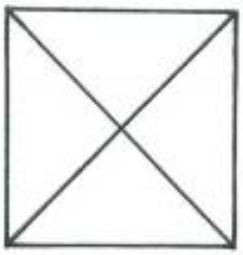

Figure 2.10: Shape of indentation of the Vickers Hardness

The definition of the Vickers hardness is that a force loaded on an indentation is dividing by an area of the indentation. The formula is showing:

$$HV = 0.009807 \times \frac{F}{S} = 0.009807 \times \frac{2F\sin\frac{a}{2}}{d^2} \quad (2\text{-}5)$$

where F is the load (kgf), d is an average value of two diagonals (mm), and a is the angle of opposite sides 136 degrees. The unit of HV is GPa after this formula calculation.

The MoAlB samples were indented by a Vickers hardness tester (2500 Knoop and Vickers tester, Buehler, Lake Bluff, IL, USA) on the top surface. The load was set as a constant value 10 kgf (9.8 N), and indenting time was 10 s. Every sample surface was indented 5 times. After indenting, the micrographs of indentation were scanning by microscope of this device. The diagonals of the indentation were measured in the micrographs. Thus, Vickers hardness of each indentation was calculated by the

Formula 2-5.

2.2.6 Oxidation resistance

The oxidation test is a corrosion test for determining oxidation resistance property of a material at high temperature with constant pressure and air compositions. Kota *et al*. tested MoAlB sample oxidation resistance at temperature 1100, 1300 and 1400 ℃, but the information of oxidation resistance at 1400 ℃ is not integrated only the composition analysis of sample surface after heating [7]. Therefore, oxidation resistance at 1400 ℃ was analyzed.

A sample with high purity 97.42 Vol. % MoAlB phase was tested at 1400 ℃. The dimension of sample was cut to 5.5 × 4.5 × 2.0 mm^3 by a diamond saw (Buehler Isomet low speed saw, Buehler, Lake Bluff, IL, USA). Figure 2.11 reveals the sample size and three faces a, b, and c marked. The Face a, Face b, and Face c are the front, left, and top. Each face of sample was ground down to 1200 grit by grinding papers, so the sample surface should be mirror-like after grinding.

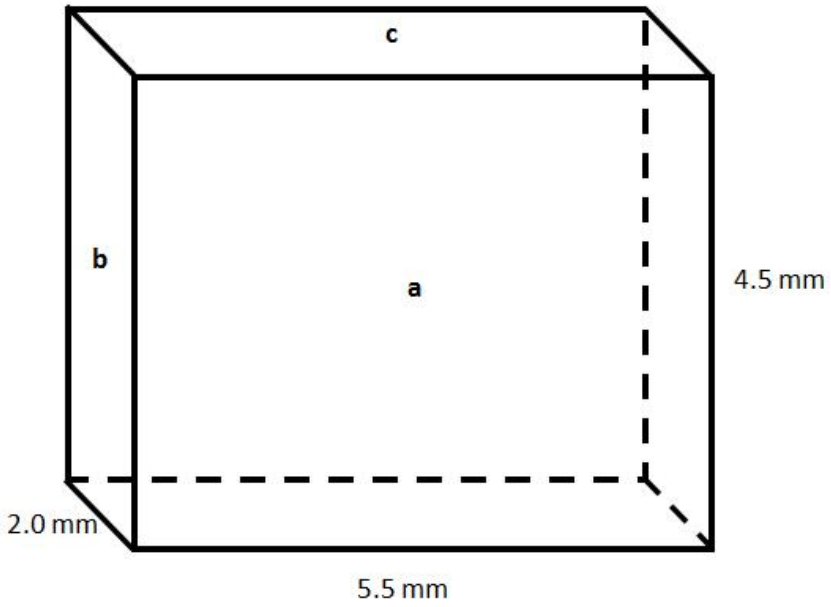

Figure 2.11: Shape of the MoAlB sample for oxidation tests

Before the oxidation test, the value of the sample mass which was keeping 4 decimal places in unit gram, which were measured by the Sartorius Secura balance (Sartorius Secura Balances S324-1S, DWS, Elk Grove, IL, USA). Besides, a high-temperature furnace (1750 ℃ Bench-Top Muffle Furnace, MTI, Richmond, CA, USA) shown in Figure 2.12 was applied in heating the MoAlB specimen. The specimen was place in the chamber of the furnace, and the Face a (5.4×4.5 mm^2) of the sample was upward. The Face a was analyzed for oxidation resistance.

Figure 2.12: High-temperature furnace

The pressure and air compositions were kept constant in the whole process of oxidation. The program of this furnace was set following the process in Table 2.2. The MoAlB specimen was heat up to 1400 ℃ with the heating rate of 10 ℃/min from the room temperature. Then temperature 1400 ℃ as the oxidation temperature was kept for 1 hour. Finally, the temperature of the chamber was cooled down to the room temperature with the rate -10 ℃/min. The sample should cool in the chamber because temperature difference could lead to cracks forming on the sample surface. In addition, there is no cooling liquid for the furnace. Thus, it should require about 12 hours for cooling sample in the furnace.

	Temperature (℃)	Heating Rate (℃/min)	Time (hour)
Initial Condition	24	0	0
Increase Temperature	1400	10	2.3
Keep Temperature	1400	0	1
Decrease Temperature	24	-10	12
Final Condition	24	0	0

Table 2.2: High-temperature furnace program of an oxidation test at 1400 ℃ for 1 hour

After finishing the first oxidation test, the sample mass should be measured and recorded. Then the second oxidation test at 1400 ℃ was repeated. The process of heating, cooling and weighting was repeated until the mass of sample remaining unchanged.

After oxidation tests at 1400 ℃, the sample surface was formed an oxide layer. The Face a of the specimen was characterized by the X-ray diffractometer. Then the X-ray diffractogram was shown by the JADE software. Finally, the element compositions of the Face a after oxidation were identified by the PDF cards.

Cross section the Face b (4.5×2.0 mm^2) was used to observe oxide scale by the SEM. The cold-mounting method was used to mount sample in a plastic cylindrical die. The specimen was placed in the middle of the mold, and the Face b was downward. Afterwards, resin and hardener were mixed in a volume ratio of 15 : 2. After stirring the mixtures homogeneously, the mixtures were poured into the cylindrical die until submerging the whole sample. Figure 2.13 demonstrates the

sample mounted in the mold. After 24 h, the sample with a mount was taken out, and the Face b was polished down to 1200 grit by grinding papers. Finally, the microstructure and compositions of the cross section was characterized by the SEM.

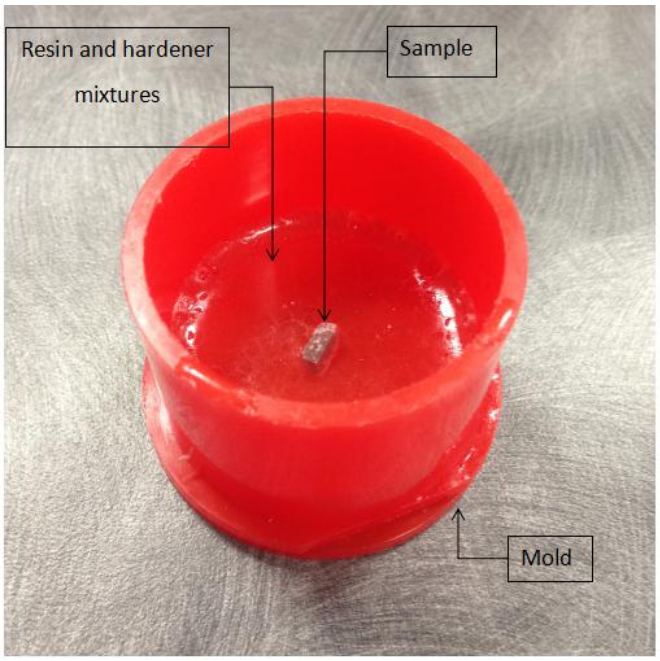

Figure 2.13: Cold-mounting method

Chapter 3: Results and Discussion

3.1 Selection of MoAlB samples in different synthesis conditions

The MoAlB samples were fabricated by the SPS with different synthesis conditions which have difference between temperature and pressure. The sintering time of the SPS 8 minutes which is referencing the SPS method of fabricating Ti_3SiC_2 by Gao *et al*. [23]. The pressure of the SPS was selected between 50 and 100 MPa. It was referring to the hot pressing method of fabricating Ti_2AlC by Cui *et al*. [18].

The optimized sintering temperature of the SPS was determined by controlling sintering time 8 minutes and pressure 50 MPa. When temperature of sintering was below 1100 ℃, the sample's purity of MoAlB is low. For example, the impurity phase was about 15 vol. % in the sample at sintering temperature 900 ℃ measured by the backscattered electron micrographs. When the temperature was at 1300 ℃, the phase of MoAlB was nonexistent in the sample, which was determined by its X-ray diffractograms and corresponding PDF cards. Thus, optimum temperature was determined in a range between 1100 and 1200 ℃.

According to above information about pressure and temperature, 4 kinds of MoAlB samples with 4 kinds of synthesis conditions were fabricated by the SPS in Table 3.1. The table lists these 4 MoAlB samples synthesized with different temperature and pressure of the SPS. Thereby, find the best synthesis condition from them.

	Sintering Time (min)	Temperature (℃)	Pressure (MPa)
Sample 1	8	1100	50
Sample 2	8	1200	50
Sample 3	8	1100	100
Sample 4	8	1200	100

Table 3.1: Samples fabricated in 4 kinds of synthesis conditions

3.2 Density analysis

The densities of 4 samples was calculated by the Formula 2-3 following the Archimedes principle in Table 3.2. Theoretical density of MoAlB is 6.45g/cm^3 [7], and samples' densities from the table were bit lower than theoretical density. The SPS system fabricated the cylindrical bulks of samples from the mixture powders, and there were some pores formed in the bulk of samples when two punches compressed powders at high temperature. Therefore, the density of each sample is lower than the theoretical density. The secondary electron micrographs will show these pores on the sample surface in the next section 3.2.

	Synthesis Condition	Density(g/cm^3)	Relative Density (%)
Sample 1	1100℃, 50MPa	5.947±0.008	92.20±0.12
Sample 2	1200℃, 50MPa	6.155±0.003	95.43±0.04
Sample 3	1100℃, 100MPa	6.186±0.006	95.90±0.09
Sample 4	1200℃, 100MPa	6.278±0.007	97.34±0.10

Table 3.2: Density and relative density of samples

The Table 3.2 lists each sample's density increasing with the temperature, so the purity of MoAlB is increasing with temperature from 1100 to 1200 ℃. It also reveals the density enlarging with pressure because high pressure can decrease the pores' sizes in the process of sintering. Thus, optimum synthesis condition of the SPS is temperature at 1200 ℃ and pressure at 100MPa. The sample 4 has optimized density value 6.278 ± 0.007 g/cm^3.

The relative density of MoAlB is also calculated in this table. The highest relative of sample 4 is 97.34 ± 0.10 %. The relative density of MoAlB is 94 ± 1% fabricated by the hot pressing method reported by Kota *et al* [7]. The sample 4's relative density by the SPS is much higher than the results by the hot pressing method.

3.3 Secondary electron micrograph

The top surface of MoAlB sample was characterized by the secondary electrons of the SEM. Figure 3.1 demonstrates the microstructure on surface of the sample 1 with 8000 magnification. There are some big and small dents on the surface. The reason of forming small dents is that grains on the surface were taken away by the grinding papers when the sample 1 was polished by grinding papers. It confirms that the MoAlB sample has low ductility. The big holes are the pores caused by the SPS fabricating bulk MoAlB samples from powders. Thus, this is the reason why samples' density lower than theoretical density. The surface topographies of the rest of samples in secondary electron micrographs are close to the sample 1's, which also have small and big dents on the top surface.

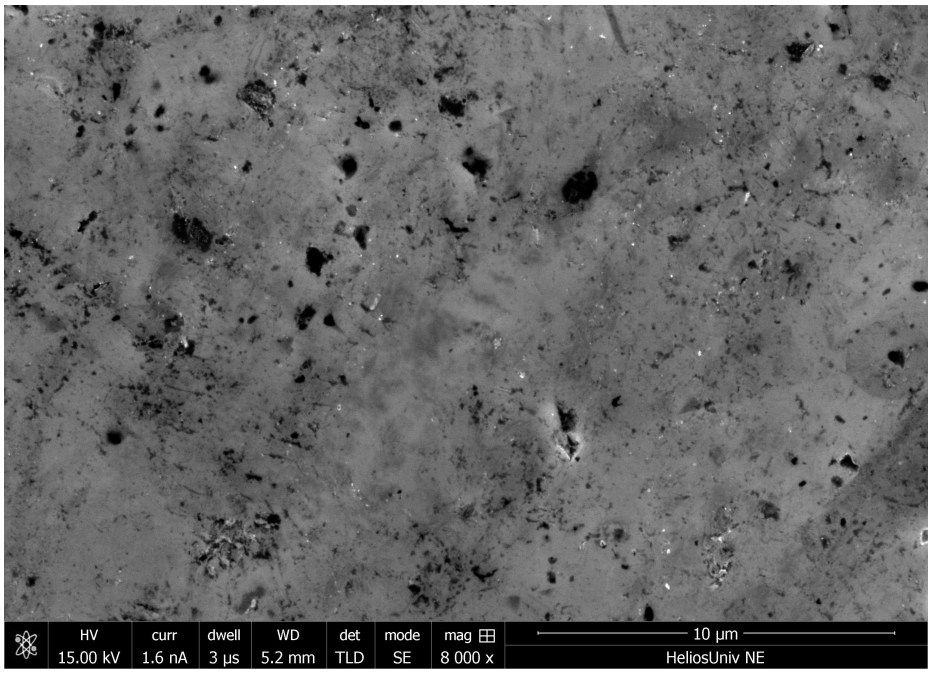

Figure 3.1: Secondary electron micrograph of sample 1's top surface

Figure 3.2 shows the secondary electron micrograph of the fracture surface of sample 1 at high magnification. The fracture surface was cracking along with grains' shape, so the fracture surface can reflected the structure of grains. The Figure 3.2 illustrates striated and layered structure of grains which are the feature of nanolaminated materials. It agrees with the results of fracture surface characterized by Kota *et al*. [7].

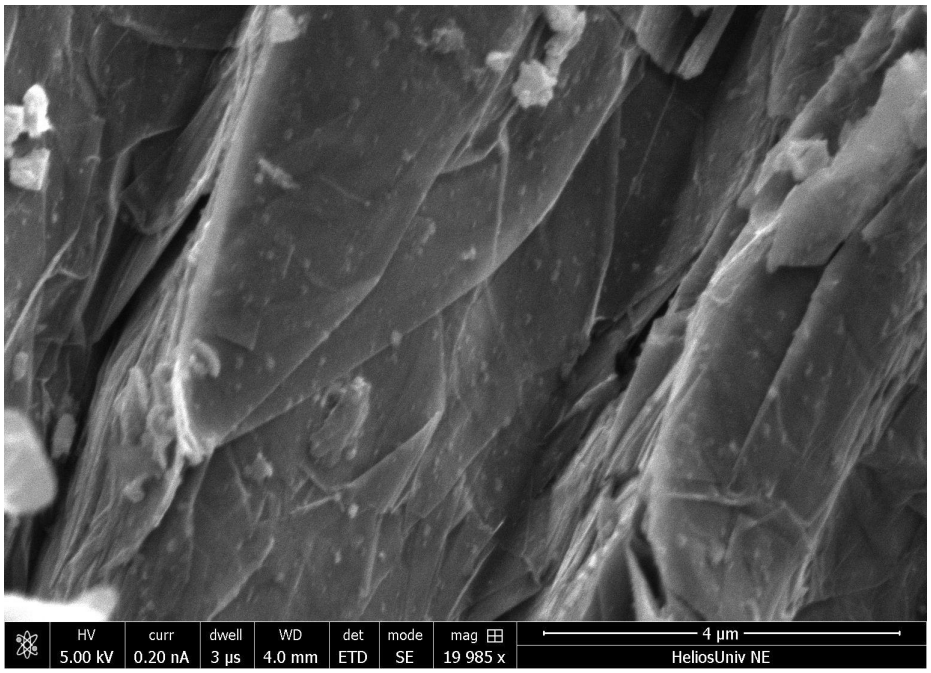

Figure 3.2: Fracture surface of sample 1 in secondary electron micrograph

3.4 Backscattered electron micrograph

Backscattered electrons were used to characterize different phases on the top surface of MoAlB samples. Five backscattered electron micrographs of different areas in each sample were taken by the SEM randomly. The volume percentage of impurities in each micrograph was calculated by a software Image J. Then mean value of the purity volume percentages was calculated in each sample. Finally, the EDS was analyzed to the atomic ratio of elements in each phase, and the EDS results as references can be used to deduce impurity compositions.

The backscattered electron micrographs of sample 1 in Figure 3.3 (a) and (b) reveals there are two phases on the top surface. The Figure 3.3 (b) with high magnification demonstrates that major phase is light gray, impurity phase is dark gray, and the dents are dark. Besides, the main phase MoAlB is 95.24 ± 1.50 vol. % of

sample 1, which is calculated by the Image J.

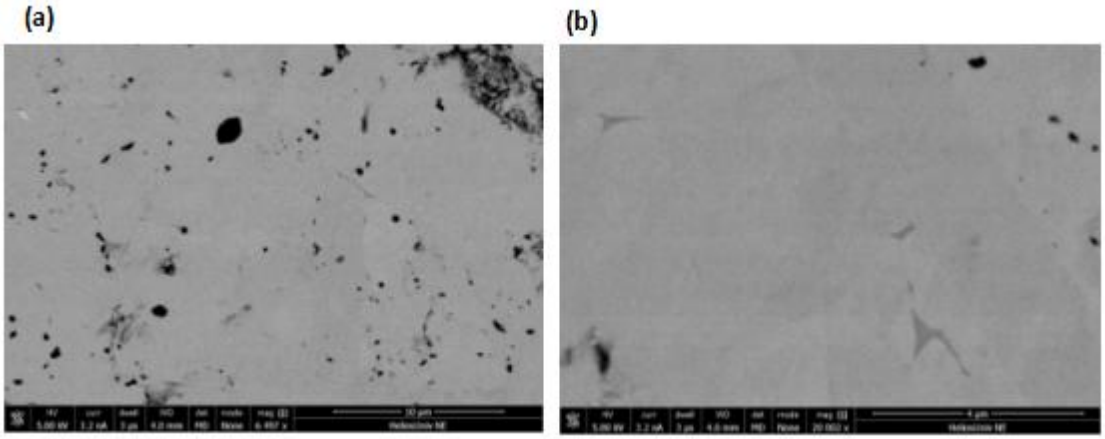

Figure 3.3: (a) Backscattered electron micrographs of sample 1 with low magnification, (b) Backscattered electron micrographs of sample 1 with high magnification

After the EDS analysis, the molar ratio of Al to Mo in major phase is close to 1 : 1, so it is the MoAlB phase. In addition, the molar ratio of Al to Mo in minor phase is 2.62 : 1. From this atomic ratio, the impurity agrees with the impurity Al_3Mo in the MoAlB sample fabricated by the hot pressing method by Kota *et al*. [7].

However, the Al-Mo phase diagram in Figure 3.4 and partial Al-Mo phase diagrams in Figure 3.5 and 3.6 reported by Saunders [24] show a different result. The Figure 3.5 shows the Al_3Mo phase confused with Al_8Mo_3 phase at the atomic 25 % Mo from 1222 to 818 ℃ [24]. Then the confused phase can convert to pure Al_8Mo_3 phase after cooling down under 818 ℃. The Figure 3.4 and the Figure 3.6 reveal that the Al_8Mo_3 (Atomic ratio: Mo:Al = 2.67 : 1) from the atomic 20 to 27.3 % Mo. The molar ratio of sample 1's impurity (Atomic ratio: Mo:Al = 2.62 : 1) is close to the phase Al_8Mo_3. Based on above information, the impurity phase which is speculated is

Al_8Mo_3.

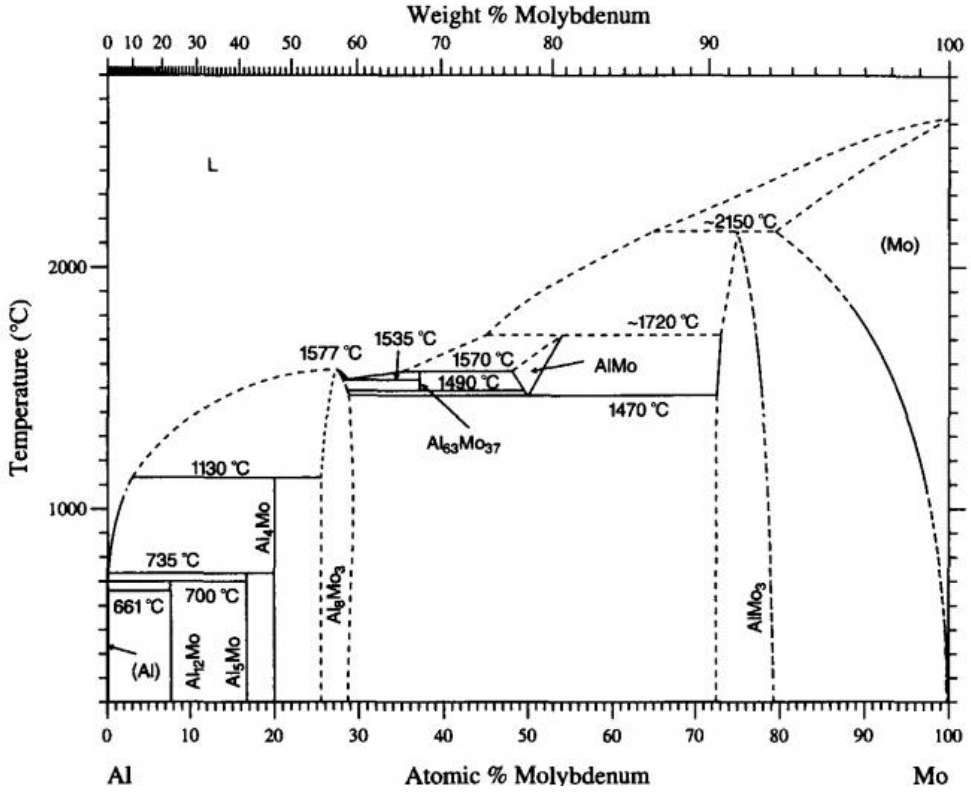

Figure 3.4: Al-Mo phase diagram [24]

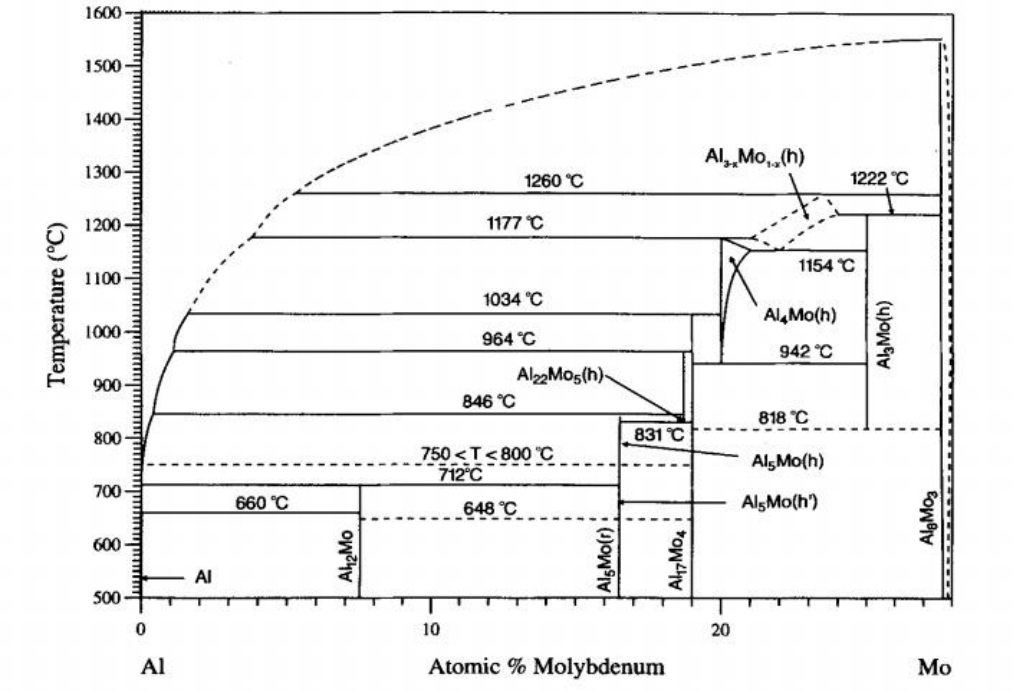

Figure 3.5: Partial Al-Mo phase diagram [24]

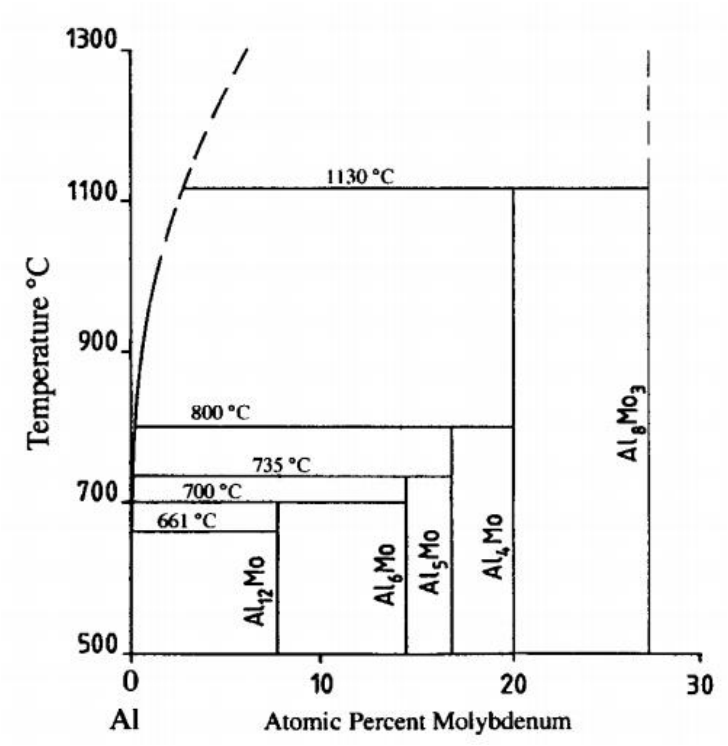

Figure 3.6: Partial Al-Mo phase diagram [24]

The sample 2's backscattered electron micrographs of Figure 3.7 (a) and (b) demonstrate there are 2 phases in the graphs and the color of impurity phase is brighter than major phase's. The major phase MoAlB is 96.25 ± 3.59 vol. % by the Image J and the EDS. The EDS results of the impurity phase demonstrate that the atomic ratio of Al to Mo is 1 : 59. It means there is no Al element in the impurity phase referring to the Al-Mo systems in Figure 3.4. The impurity phase most likely to be the MoB.

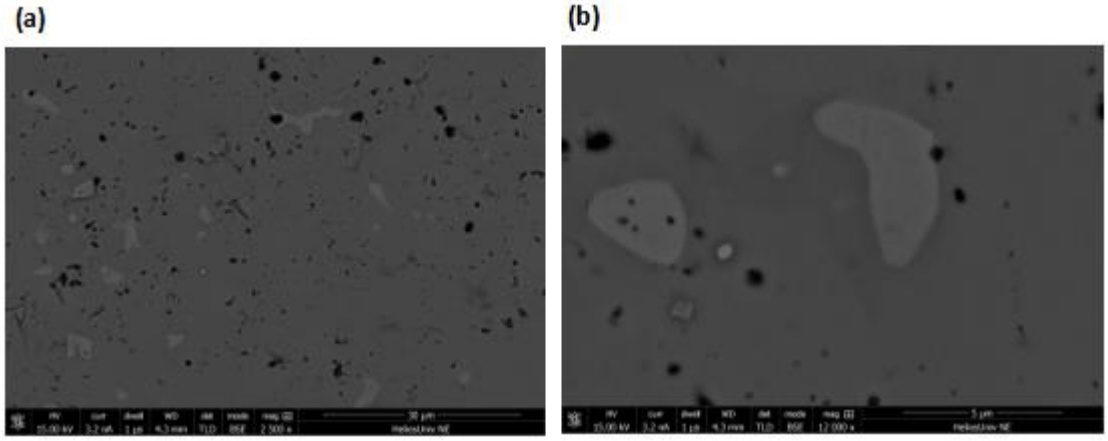

Figure 3.7: (a) Backscattered electron micrographs of sample 2 with low magnification, (b) Backscattered electron micrographs of sample 2 with high magnification

The backscattered electron micrographs of sample 3 in Figure 3.8 (a) and (b) illustrate light gray MoAlB phase and dark gray impurities phase. The MoAlB phase is 97.42 ± 1.48 vol. % of sample 3, so the purity of MoAlB is high in sample 3. The EDS results reveal the atomic ratio of Al to Mo is 2.53 : 1. According to the Al-Mo phase diagram in Figure 3.4, the impurity phase could be Al_8Mo_3.

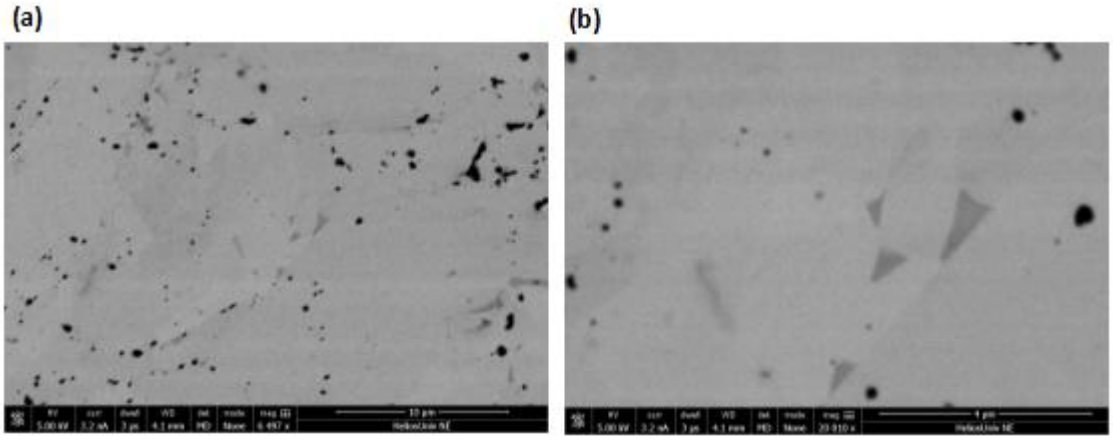

Figure 3.8: (a) Backscattered electron micrographs of sample 3 with low magnification, (b) Backscattered electron micrographs of sample 3 with high magnification

Figure 3.9 (a) and (b) illustrate 2 phases in backscattered electron micrographs of sample 4. Light gray phase is MoAlB, and dark gray phase is impurity phase by using the EDS analysis. After calculation, the sample 4 has highest MoAlB phase 98.03 ± 0.98 vol. %. The impurity phase could be Al_8Mo_3 because the ratio of Al to Mo is 2.45 : 1 by the EDS analysis.

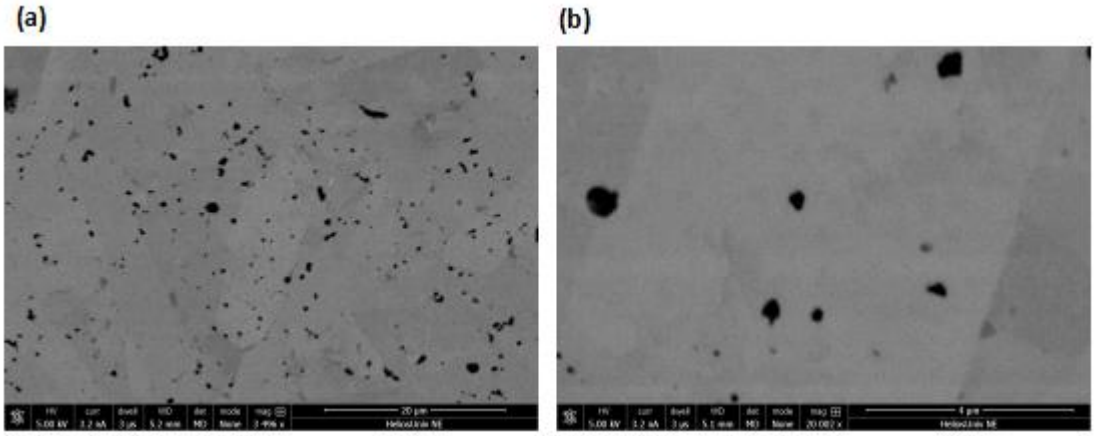

Figure 3.9: (a) Backscattered electron micrographs of sample 4 with low magnification, (b) Backscattered electron micrographs of sample 4 with high magnification

Table 3.3 summarizes the results of the backscattered electron micrographs and the EDS. The purity of MoAlB is increasing with temperature and pressure in a partial range. The results of purity are same with the results of density, which is also increasing with temperature and pressure in Table 3.3. The highest purity is 98.03 ± 0.98 vol. % in the synthesis condition 1200 ℃ and 100MPa, it is the best synthesis condition of the SPS. Besides, the results of impurities composition analysis are also shown in this table. The volume percentage of impurity in each sample is low, so it is not an important factor to affect property measurements for MoAlB samples.

	Synthesis Condition	Probable Impurity Composition	MoAlB Vol.%
Sample 1	1100℃, 50MPa	Al_8Mo_3	95.24±1.50
Sample 2	1200℃, 50MPa	MoB	96.25±3.59
Sample 3	1100℃, 100MPa	Al_8Mo_3	97.42±1.48
Sample 4	1200℃, 100MPa	Al_8Mo_3	98.03±0.98

Table 3.3: Volume percentage and impurity probable composition of sample

3.5 X-ray diffractogram

The XRD is another method to analyze compositions of each sample. The diffraction peaks in the X-ray diffractograms are compared to the standard X-ray diffraction patterns (PDF cards). From the results of the EDS, the impurity compositions could be confirmed from diffraction peaks in each sample. However, the compositions of impurities are in small volume percentage. Thus, the diffraction peaks of impurities are hardly observed in each diffractogram. Therefore, the X-ray diffractograms reveal the diffraction peaks belong to MoAlB phase.

The diffraction peaks of 4 MoAlB samples are almost same because every sample has high purity of MoAlB phase. The X-ray diffractogram of sample 1 are used to analyze in Figure 3.10, and other 3 samples' diffractograms are in Chapter 5 Appendix. The diffraction peaks of the sample 1 are compared to the standard X-ray diffraction pattern which is at the bottom of the Figure 3.10. Each peak position in the diffractogram was labeled as corresponding plane {h k l} of MoAlB by referring its

PDF card.

The results of the Figure 3.10 reveal all diffraction peaks are belong to MoAlB phase. Besides, intensities of diffraction peaks in {0k0} peak positions are a bit higher than peak intensities of the standard X-ray diffraction pattern. It is an agreement with the results of the hot-pressed MoAlB sample on the top face reported by by Kota *et al*. [7]. It confirms that the SPS can promote the MoAlB crystal growing preferentially in the {0k0} axis on the top surface.

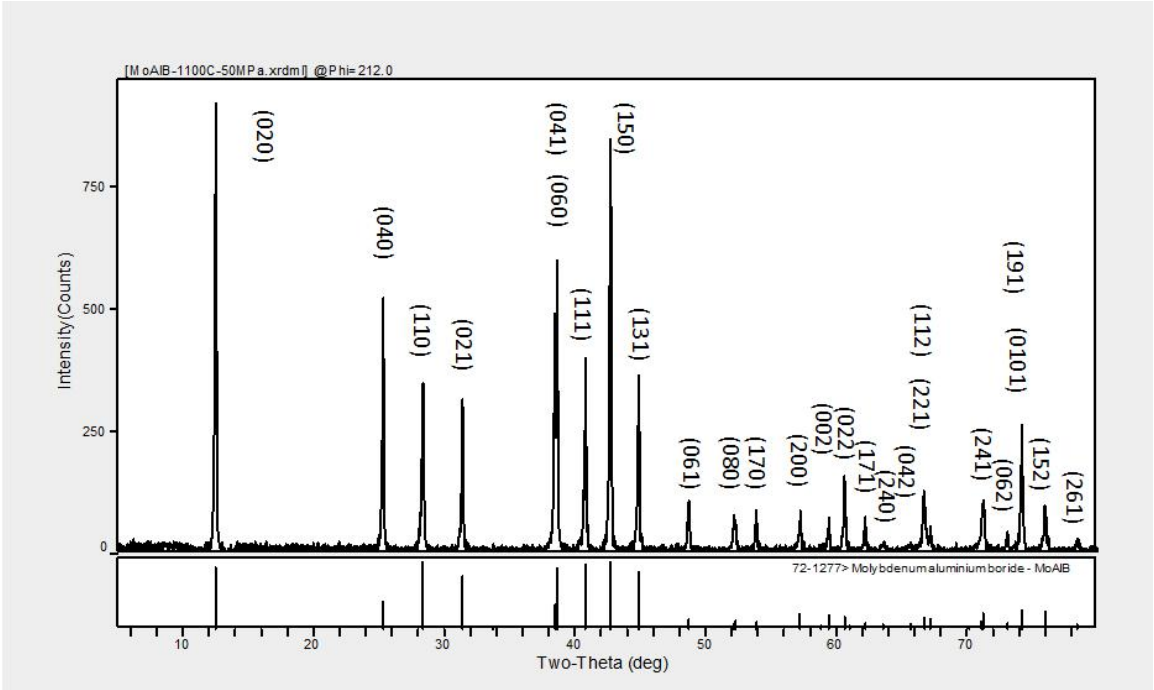

Figure 3.10: X-ray diffractograms of MoAlB sample 1 on the top surface and diffraction peaks of MoAlB standard X-ray diffraction pattern

3.6 Vickers hardness

The Vickers hardness of each indentation was calculated by the Formula 2-5, and each sample had 5 indentations. The Vickers hardness mean value of each sample with a constant force 9.8 N is revealed in Table 3.4. The results shows the Vickers

hardness values of samples in different synthesis conditions are close. It is the value between 10.48 and 10.74 GPa. The results agree with the MoAlB polycrystal on the cross-section 10.6 ± 0.3 GPa by Kota *et al*. [7] and MoAlB single crystal on the b-plane 10.3 ± 0.2 GPa by Okada [13]. The hardness of binary counterpart molybdenum boride (MoB) is 23 GPa [14], so the hardness value is decreasing when binary counterpart forming a nanolaminated structure. The metallic bond Mo-Al is weaker than the covalent bond B-B and the ionic bond Mo-B.

	Synthesis Condition	Force (N)	Vickers Hardness (GPa)
Sample 1	1100℃, 50MPa	9.8	10.60±0.51
Sample 2	1200℃, 50MPa	9.8	10.75±0.36
Sample 3	1100℃, 100MPa	9.8	10.64±0.65
Sample 4	1200℃, 100MPa	9.8	10.48±0.41

Table 3.4: Vickers hardness of each sample

The indentations of 4 samples shown in Figure 3.11 are exactly similar. There are some small cracks at the borders of indentations with the maximum load of 9.8 N. However, the small cracks are not dominant. Thus, the nanolaminated structure of MoAlB can reduce the formation of cracks when the samples are indente. Therefore, the MoAlB ceramics have better damage tolerance.

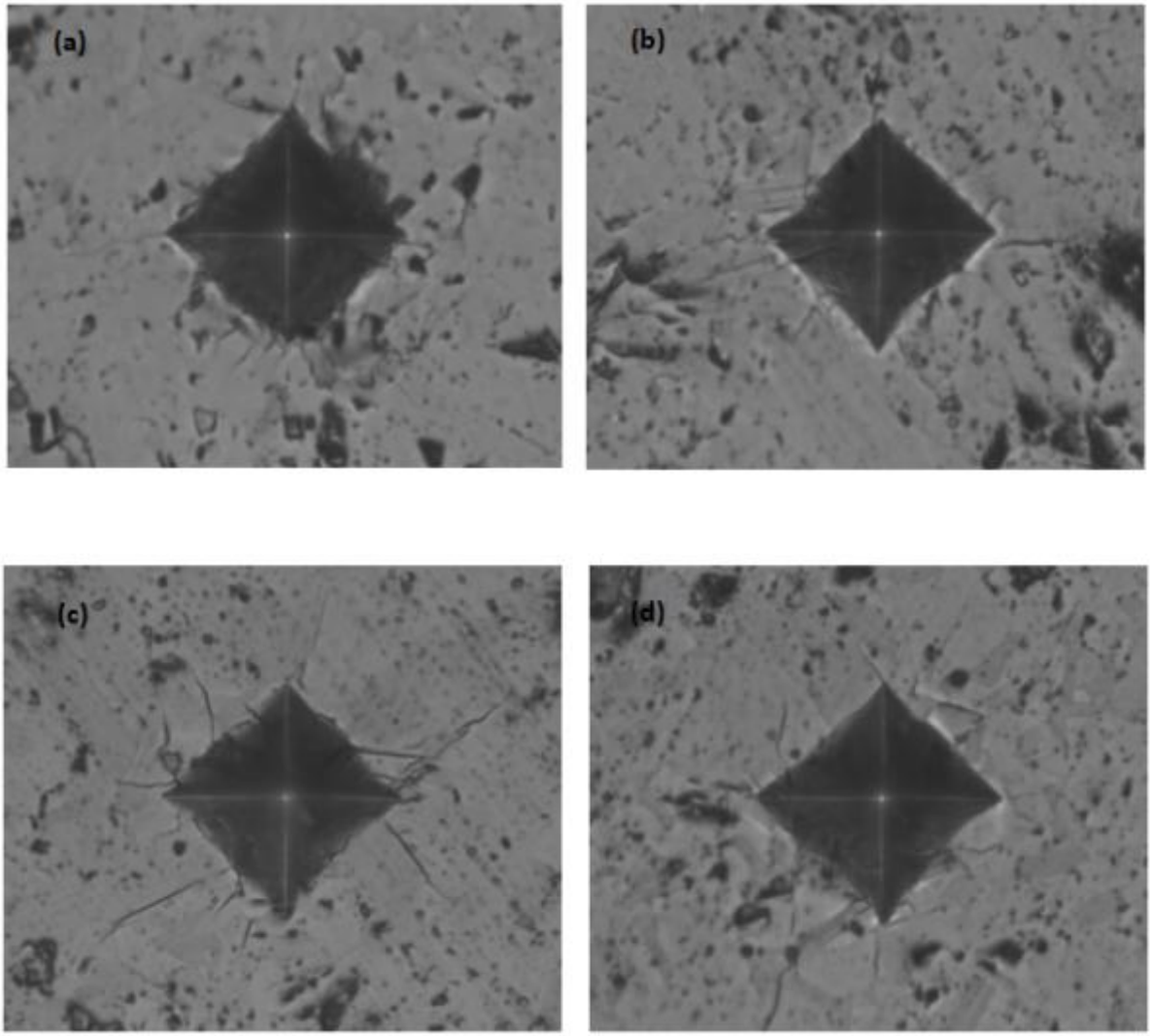

Figure 3.11: (a) Indentation of sample 1, (b) Indentation of sample 2, (c) Indentation of sample 3, and (d) Indentation of sample 4

3.7 Oxidation resistance

The sample 3 with high purity 97.42 Vol. % was used for oxidation tests at 1400 ℃. The value of the sample mass was recorded after each oxidation test with 1 h, and the mass stopped increasing after the seventh test (7 hours). Then the relation between the increase of mass and the time of oxidation at 1400 ℃ for 7 hours was analyzed. The parabolic relation is between Δm/A and t at 1400 ℃ in Figure 3.12. The Δm is the difference value between the mass after oxidation test and the initial

mass (kg), A is the area of the Face a ($0.0054 \times 0.0045\ m^2$), and t is the time of oxidation (hour).

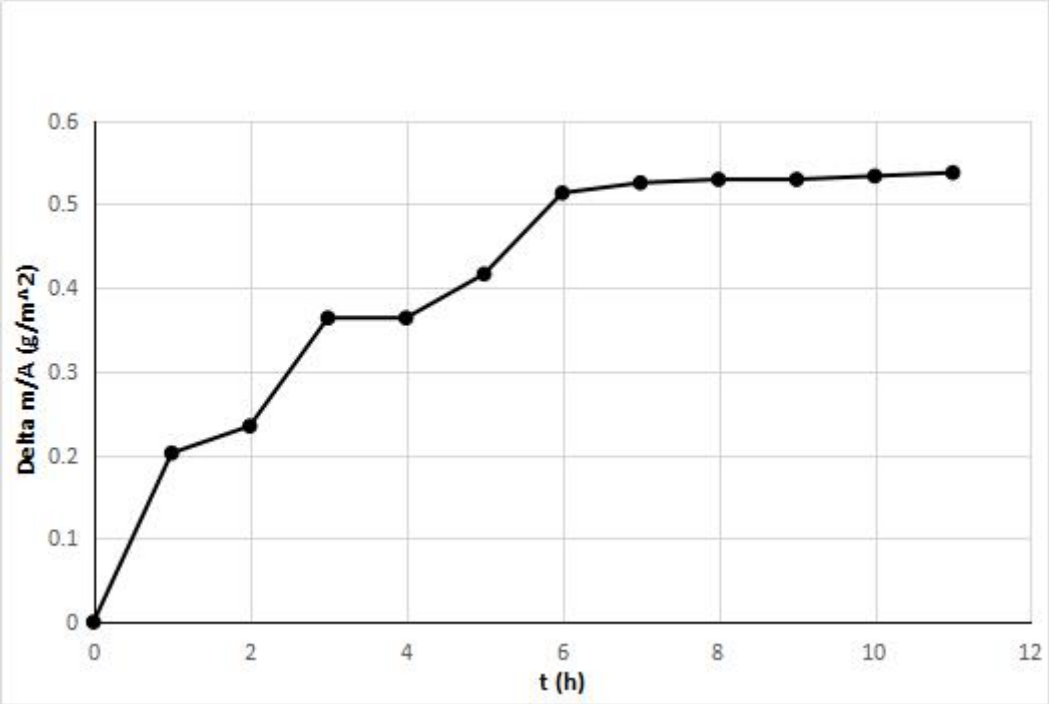

Figure 3.12: Δm/A increase with t (0< t <8)

Then Figure 3.13 illustrates linear relation between $(\Delta m/A)^2$ and t at 1400 ℃ by equation:

$$\left(\frac{\Delta m}{A}\right)^2 = Ct, \ (0< t <8) \tag{3-1}$$

where C is a constant number 0.0387 $kg^2/(hm^4)$. The constant number C at 1400 ℃ is determined by the data in the graph with a good power law fit ($R^2 = 0.9449$). Finally, transfer the Formula 3-1 to the parabolic rate law, and get the equation:

$$(\Delta m)^2 = 2.37 \times 10^{-11}\, t, (0 < t < 8). \tag{3-2}$$

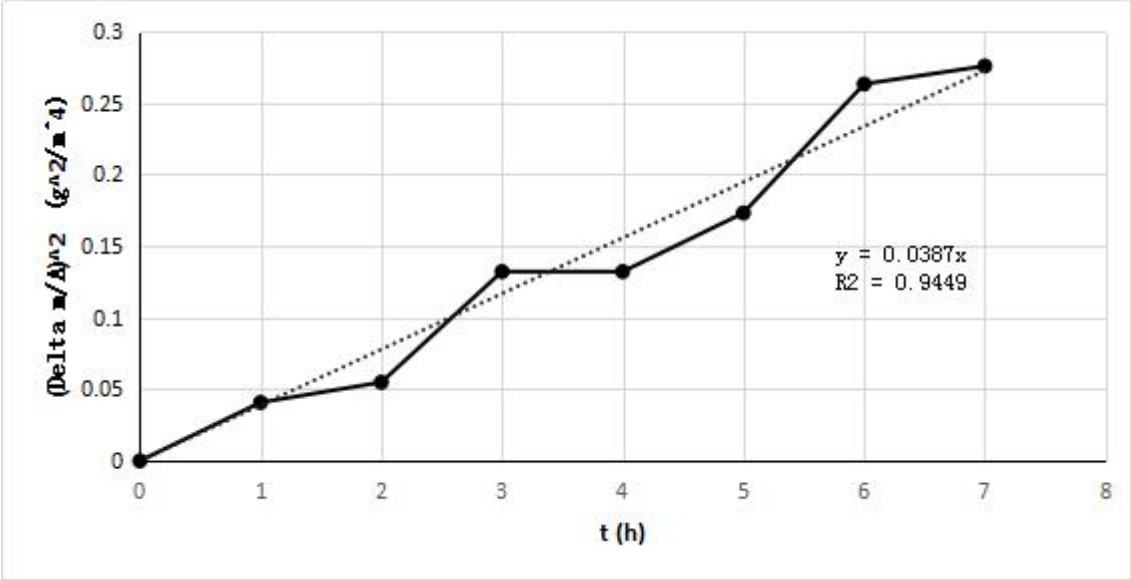

Figure 3.13: (Δm/A) 2 is linear to t (0< t <8)

Figure 3.14 is the X-ray diffractogram of the sample 3 after oxidation at 1400 ℃ for 11 h. It reveals that peaks with high intensities are belonging to the Al_2O_3 phase and weak peaks are belonging to MoB and MoAlB phases. The results confirm that major phase on the Face a is Al_2O_3 and minor phases are MoB and MoAlB. Based on above evidences of elemental compositions after oxidation tests, the oxidation reaction is:

$$MoAlB + \frac{3}{4}O_2 \rightarrow MoB + \frac{1}{2}Al_2O_3 \quad (T = 1400\ ℃). \qquad (3\text{-}3)$$

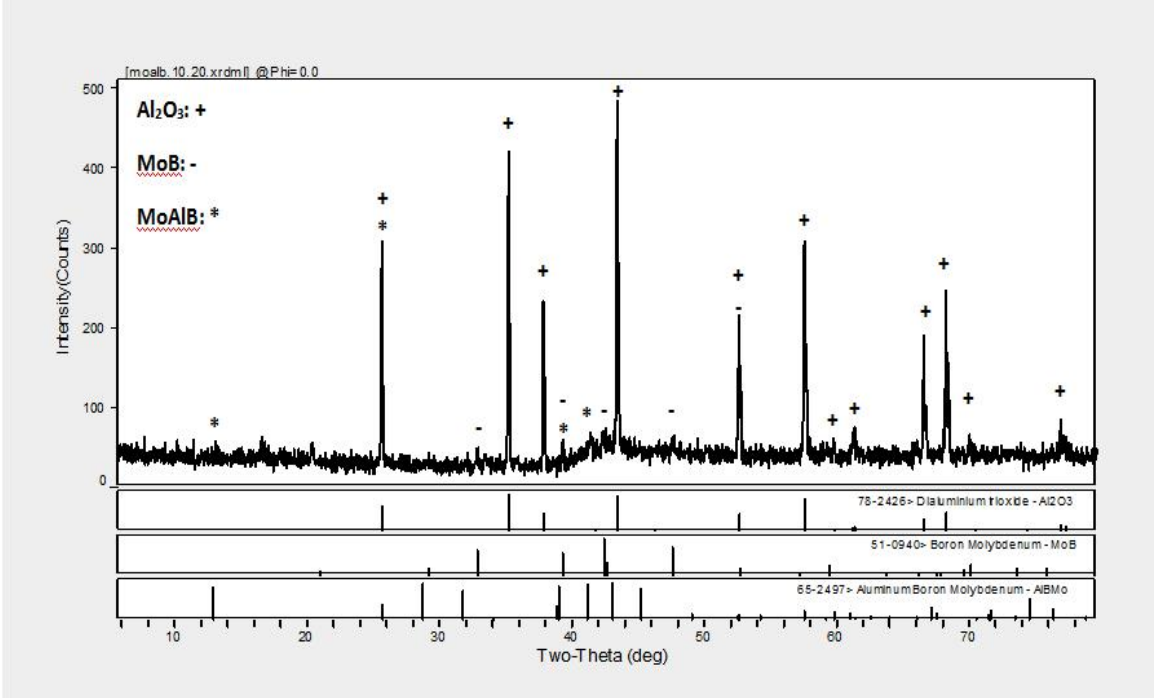

Figure 3.14: X-ray diffractograms of the sample 3 after oxidation at 1400 ℃ for 11 h

The cross section (Face b) after oxidation tests was characterized by the SEM. The secondary electron micrograph with low magnification (Figure 3.5) reveals the boundary between the sample's cross section and the resin. There are three regions resin phase (a), Al_2O_3 phase (b), and mixed phases (c) in the micrograph.

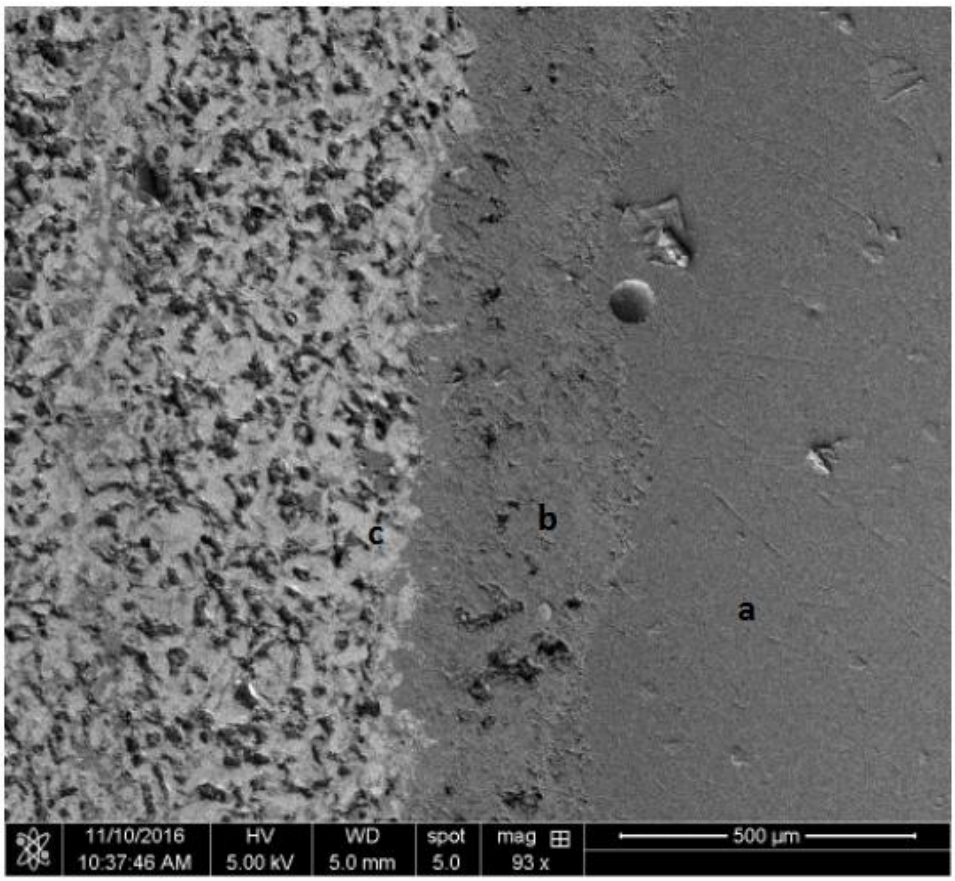

Figure 3.15: Secondary electron micrograph with low magnification of the cross section's boundary showing 3 significant regions

In order to analyze the mixed phases, the backscattered electron micrograph of alumina scale boundary was taken in Figure 3.16. It shows there are 4 phases at the interface between the region of mixture phases and alumina scale. The EDS results of the Figure 3.16 show that phase a is Al_2O_3, phase b is MoAlB, phase c is the impurity phase Al_8Mo_3, and phase d is MoB. Thereby, the Al_2O_3 phase and MoB phase are inserting in the region of MoAlB phase. It causes the mixed phases in the region a in the Figure 3.15.

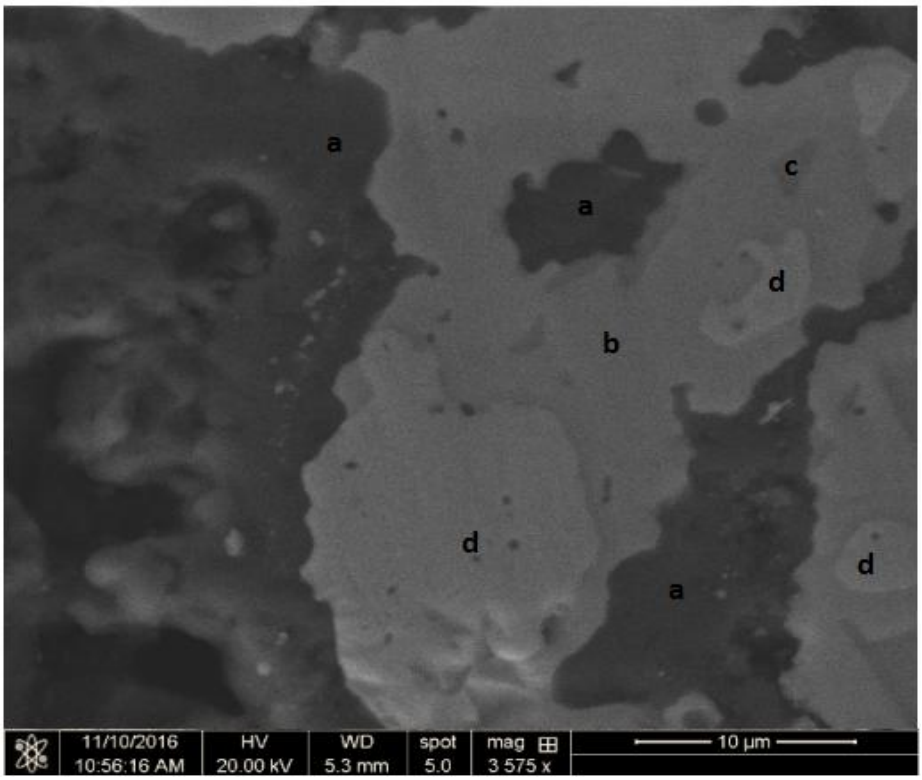

Figure 3.16: Backscattered electron micrograph of cross section interface

The backscattered electron micrograph in Figure 1.13 shows that the cross section for 200 h at 1300 ℃ has a pure MoAlB region by Kota *et al*. [7]. However, the MoAlB phase is mixed with MoB phase and Al_2O_3 phase in the Figure 3.16. Continue to do oxidation at 1400 ℃ for 2 hours to observe micrographs of mixed region.

Chapter 4. Conclusions

The polycrystal MoAlB samples were synthesized from MoB and Al powders by using the SPS method. The optimum sintering temperature and pressure values are 1200 ℃ and 100 MPa with a sintering time of 8 minutes.

The sample has a high relative density of 97.34 ± 0.10 % and a high purity of 98.03 ± 0.98 vol. %. The impurity composition could be Al_8Mo_3 by the EDS analysis. The XRD can analyze high purity of MoAlB composition because almost all peaks in the X-ray diffractogram belong to MoAlB phase.

There are some pores in the bulk of MoAlB samples, and they are caused by using the SPS method to fabricate samples. Besides, striated and layered structure of grains can be observed by the SEM.

The Vickers hardness value is 10.48 ± 0.41 GPa, and there are no dominate crack along the edge of the indentations. The Mo-Al bonds in the MoAlB sample can decrease the Vickers hardness value which is comparing with its binary counterparts; besides, the nanolaminated structure can make MoAlB samples have the property of mechanical damage tolerance.

The results of oxidation tests confirm that the MoAlB sample is stable at 1400 ℃. The sample can form alumina layer and mixed layer at 1400 ℃ for 11 h. The mixed layer contains the Al_2O_3 phase and the MoB phase inserting in the region of the MoAlB phase.

Chapter 5: Appendix

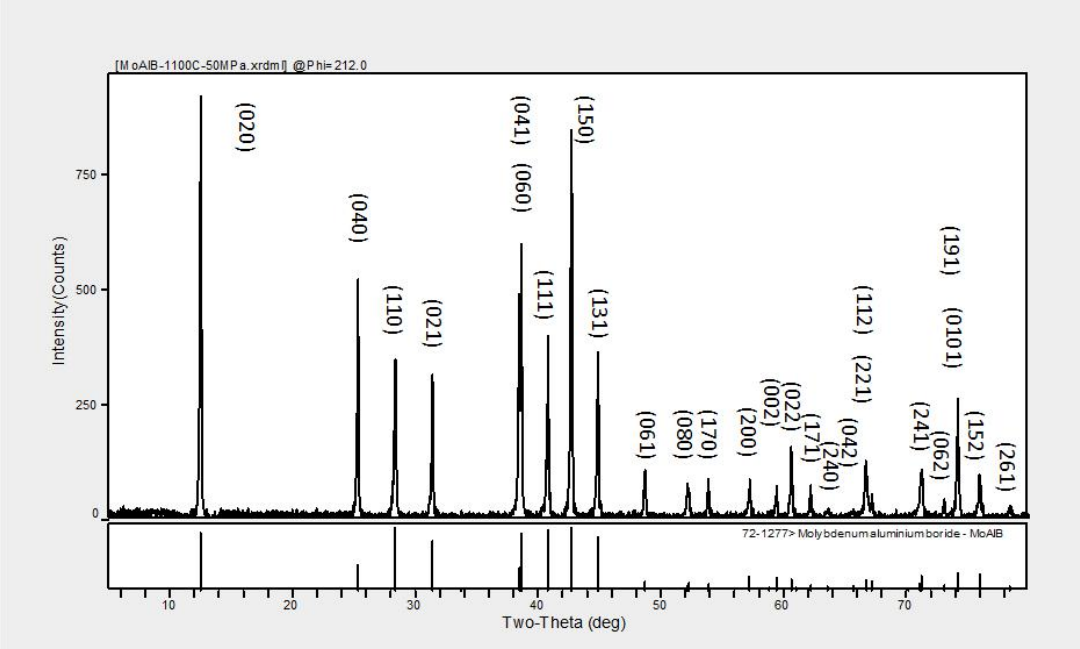

Figure 5.1: X-ray diffractograms of the MoAlB sample 1 on the top surface

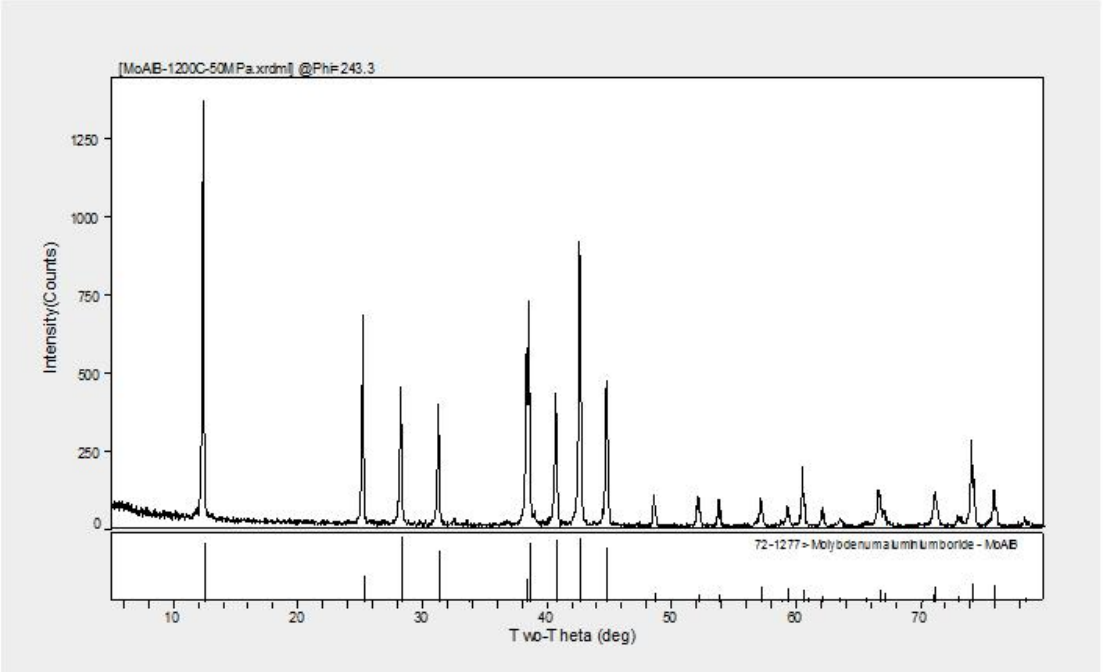

Figure 5.2: X-ray diffractograms of the MoAlB sample 2 on the top surface

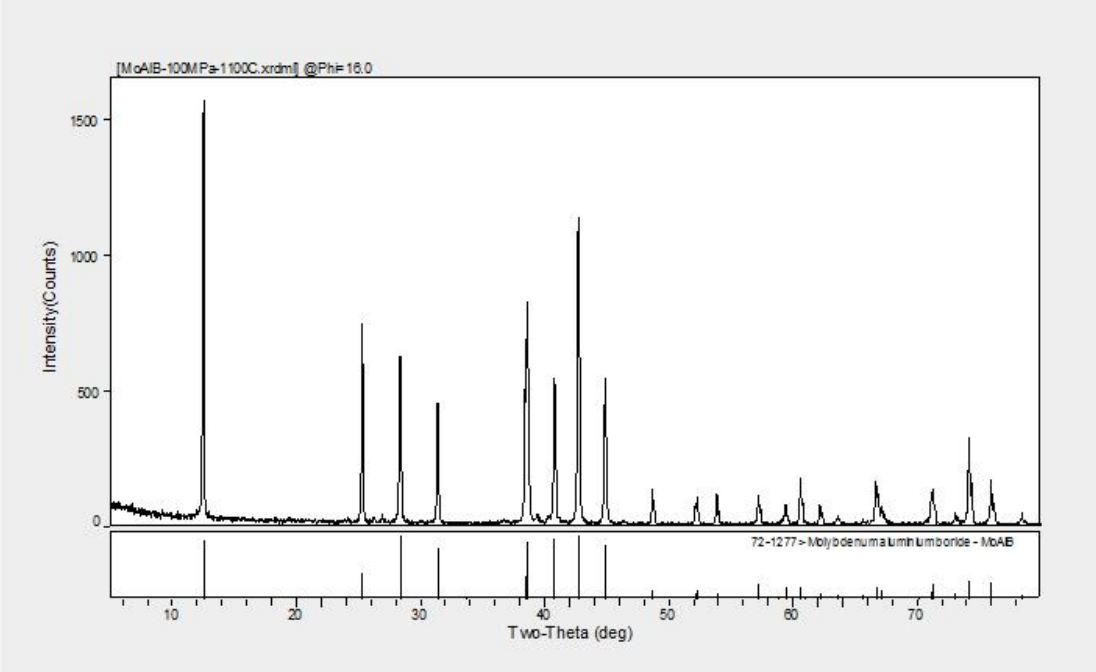

Figure 5.3: X-ray diffractograms of the MoAlB sample 3 on the top surface

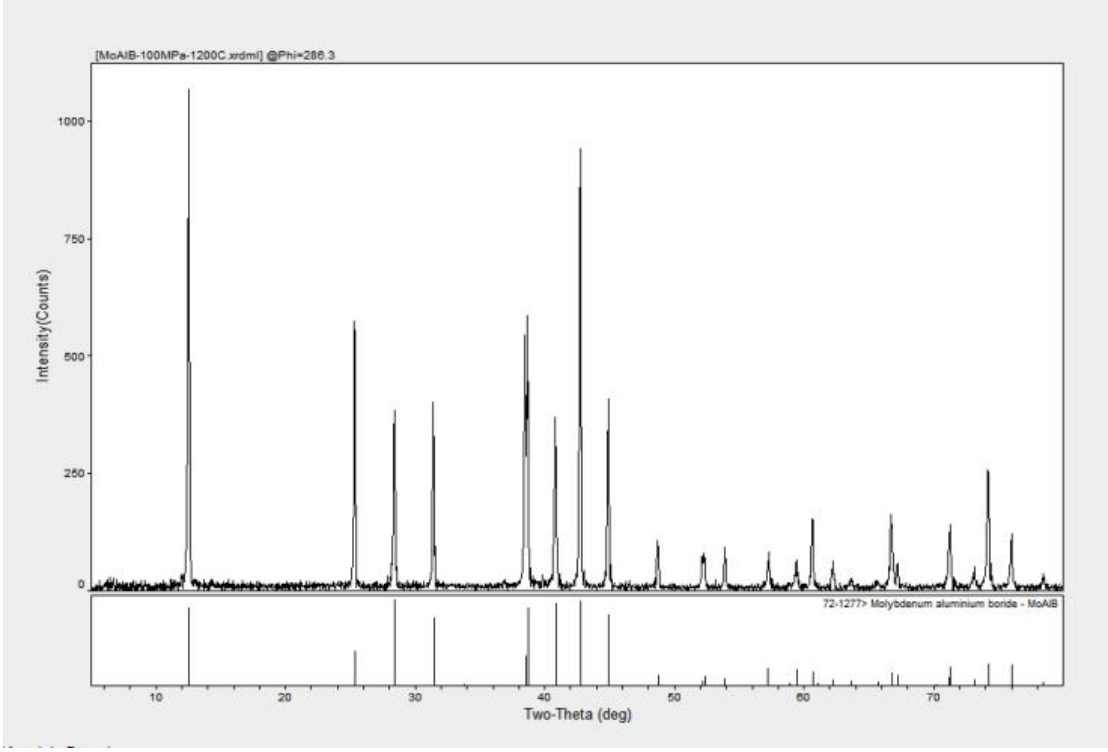

Figure 5.4: X-ray diffractograms of the MoAlB sample 4 on the top surface

Chapter 6. References

[1] Martini, C., Palombarini, G., Poli, G. & Prandstraller, D. Sliding and abrasive wear behaviour of boride coatings. *Wear* 256, 608–613 (2004).

[2] Yu, X. W. & Licht, S. A novel high capacity, environmentally benign energy storage system: Super-iron boride battery. *J. Power Sources* 179, 407-411 (2008).

[3] Licht, S., Yu, X. & Qu, D. A novel alkaline redox couple: chemistry of the Fe(6+)/B(2−) super-iron boride battery. *Chem. Commun.*(*Camb*). 2, 2753–5 (2007).

[4] Aylett, B. J. Borides & Silicides–New Chemistry and Applications. *Br. Polym. J.* 18, 359–363 (1986).

[5] Okada, S., Kudou, K. & Shishido, T. Synthesis and some properties of molybdenum diboride MoB_2. *Pac. Sci .Rev*. 11, 164–171 (2011).

[6] Okada, S. Synthesis, Crystal Structure and Characterizations of the Ternary Borides TMAlB (TM=Mo,W) with UBC Type Structure. *Trans. Kokushikan Univ. Fac. Eng*. 7–12 (1998).

[7] Kota, S., Zapata-Solvas, E., Ly, A., Lu, J., Elkassabany, O., Huon, A., Barsoum, M. W. Synthesis and Characterization of an Alumina Forming Nanolaminated Boride: MoAlB. *Scientific Reports, 6*, 26475 (2016).

[8] Jeitschko, W. Die Kristallstruktur von MoAlB. *Monatshefte für Chemie und verwandte Teile anderer Wissenschaften* 97, 1472–1476 (1966).

[9] L. Toth, H. Nowotny, F. Benesovsky and E. Rudy, *Mh. Chem.*, 92 (1962) 794.

[10] Generalic, Eni. "Base-centered orthorhombic lattice." *Croatian-English Chemistry Dictionary & Glossary*. 15 Dec. 2015. KTF-Split. 20 Oct. 2016. <http://glossary.periodni.com>.

[11] DoITPoMS - TLP Library Atomic Scale Structure of Materials. (2004, March/April). Retrieved October 21, 2016, from http://www.doitpoms.ac.uk/tlplib/atomic-scale-structure/intro.php

[12] Ade, M. & Hillebrecht, H. Ternary Borides Cr_2AlB_2 , Cr_3AlB_4 , and Cr_4AlB_6: The First Members of the Series $(CrB_2)_nCrAl$ with n= 1, 2, 3 and a Unifying Concept for Ternary Borides as MAB-Phases. *Inorg. Chem.* 54, 6122–6135 (2015).

[13] Okada, S. *et al.* Single Crystal Growth of $(Mo_xCr_{1-x})AlB$ and $(Mo_xW_{1-x})AlB$ by Metal Al Solutions and Properties of the Crystals. *J. Solid State*

Chem. 133, 36–43 (1997).

[14] Campbell, I. E. & Sherwood, E. M. in *High Temp. Mater. Technol. 1st Edn*, Ch. 13, 360–363 (Wiley, 1967).

[15] Tao, Q. *et al*. Enhanced Vickers hardness by quasi-3D boron network in MoB_2. *RSC Adv*. 3, 18317 (2013).

[16] Monteverde, F., Bellosi, A., & Guicciardi, S. (2002). Processing and properties of zirconium diboride-based composites. *Journal of the European Ceramic Society, 22*(3), 279-288. doi:10.1016/s0955-2219(01)00284-9

[17] Desai, P. D., Chu, T. K., James, H. M. & Ho, C. Y. Electrical Resistivity of Selected Elements. *J. Phys. Chem. Ref. Data* 13, 1069 (1984).

[18] Cui, B., Jayaseelan, D. D., & Lee, W. E. Microstructural evolution during high-temperature oxidation of Ti2AlC ceramics. *Acta Materialia, 59*(10), 4116-4125 (2011).

[19]A., & Heath, T. L. (1897). *The works of Archimedes*. Cambridge: University Press.

[20] Kieffer, W. F. (1975). CRC Handbook of Chemistry and Physics. 54th Edition. *Journal of Chemical Education, 52*(2). doi:10.1021/ed052pa142.1

[21] University of Nebraska-Lincoln | Web Developer Network. (n.d.). Scanning Electron Microscope (SEM). Retrieved November 06, 2016, from http://ncmn.unl.edu/enif/microscopy/SEM.shtml

[22] Site Links. (n.d.). Retrieved November 06, 2016, from http://www.gordonengland.co.uk/hardness/vickers.htm

[23] Gao, N., Li, J., Zhang, D., & Miyamoto, Y. (2002). Rapid synthesis of dense Ti3SiC2 by spark plasma sintering. *Journal of the European Ceramic Society, 22*(13), 2365-2370. doi:10.1016/s0955-2219(02)00021-3

[24] Saunders, N. (1997). The Al-Mo system (aluminum-molybdenum). *Journal of Phase Equilibria, 18*(4), 370-378. doi:10.1007/s11669-997-0063-1